The Plant Cell, Vol. 26: 1645–1665, April 2014, www.plantcell.org

Choreography of Transcriptomes and Lipidomes of *Nannochloropsis* Reveals the Mechanisms of Oil Synthesis in Microalgae[W][OPEN]

Jing Li,[a,b,1] Danxiang Han,[c,1] Dongmei Wang,[a,1] Kang Ning,[a,1] Jing Jia,[a,b] Li Wei,[a,b] Xiaoyan Jing,[a] Shi Huang,[a,b] Jie Chen,[a] Yantao Li,[d] Qiang Hu,[e,2] and Jian Xu[a,2,3]

[a] Single-Cell Center, CAS Key Laboratory of Biofuels and Shandong Key Laboratory of Energy Genetics, Qingdao Institute of BioEnergy and Bioprocess Technology, Chinese Academy of Sciences, Qingdao, Shandong 266101, China
[b] University of Chinese Academy of Sciences, Beijing 100049, China
[c] Laboratory for Algae Research and Biotechnology, Department of Applied Biological Sciences, Arizona State University, Mesa, Arizona 85212
[d] Institute of Marine and Environmental Technology, University of Maryland Center for Environmental Science and University of Maryland Baltimore County, Baltimore, Maryland 21202
[e] Center for Microalgal Biotechnology and Biofuels, Institute of Hydrobiology, Chinese Academy of Sciences, Wuhan, Hubei 430072, China

To reveal the molecular mechanisms of oleaginousness in microalgae, transcriptomic and lipidomic dynamics of the oleaginous microalga *Nannochloropsis oceanica* IMET1 under nitrogen-replete (N+) and N-depleted (N-) conditions were simultaneously tracked. At the transcript level, enhanced triacylglycerol (TAG) synthesis under N- conditions primarily involved upregulation of seven putative diacylglycerol acyltransferase (DGAT) genes and downregulation of six other DGAT genes, with a simultaneous elevation of the other Kennedy pathway genes. Under N- conditions, despite downregulation of most de novo fatty acid synthesis genes, the pathways that shunt carbon precursors from protein and carbohydrate metabolic pathways into glycerolipid synthesis were stimulated at the transcript level. In particular, the genes involved in supplying carbon precursors and energy for de novo fatty acid synthesis, including those encoding components of the pyruvate dehydrogenase complex (PDHC), glycolysis, and PDHC bypass, and suites of specific transporters, were substantially upregulated under N- conditions, resulting in increased overall TAG production. Moreover, genes involved in the citric acid cycle and β-oxidation in mitochondria were greatly enhanced to utilize the carbon skeletons derived from membrane lipids and proteins to produce additional TAG or its precursors. This temporal and spatial regulation model of oil accumulation in microalgae provides a basis for improving our understanding of TAG synthesis in microalgae and will also enable more rational genetic engineering of TAG production.

INTRODUCTION

Microalgae are capable of storing energy in the form of triacylglycerol (TAG) under adverse environmental conditions, such as nutrient deprivation (Hu et al., 2008; Merchant et al., 2012). The high growth potential and oil content, as much as 60% of cell dry weight, of many oleaginous microalgae has led to growing interest worldwide in utilizing these organisms as a source of biomass feedstock for biofuels and biomaterials (Hu et al., 2008). As vigorous growth and TAG accumulation are usually mutually exclusive in naturally occurring microalgae, methods of genetically engineering microalgae for improved growth while stimulating TAG production have long been sought. However, the molecular and cellular mechanisms underlying lipid metabolism in microalgae are largely unknown. Identifying the pathways and regulatory networks that underlie the oleaginous phenotype should guide the rational genetic engineering of microalgae for the overproduction of TAG (Li et al., 2010a, 2010b; Georgianna and Mayfield, 2012).

As in vascular plants, it is generally thought that TAG is synthesized via two pathways in eukaryotic microalgae: the acyl-CoA dependent Kennedy pathway and the acyl-CoA independent alternative pathway mediated by a phospholipid:diacylglycerol acyltransferase (PDAT). In the Kennedy pathway, activated fatty acids (FAs) in the form of acyl-CoA are sequentially incorporated into glycerol-3-phosphate to produce TAGs, which are catalyzed by a glycerol-3-phosphate acyltransferase (GPAT), lysophosphatidic acid acyltransferase (LPAAT), phosphatidic acid phosphatase (PAP), and diacylglycerol acyltransferase (DGAT) (Coleman and Lee, 2004; Ohlrogge and Browse, 1995). Enzymes of the Kennedy pathway are often encoded by multiple copies of genes or are distinct proteins in eukaryotes (Coleman and Lee,

[1] Co-first authors
[2] These authors contributed equally to this work
[3] Address correspondence to xujian@qibebt.ac.cn.
The author responsible for distribution of materials integral to the findings presented in this article in accordance with the policy described in the Instructions for Authors (www.plantcell.org) is: Jian Xu (xujian@qibebt.ac.cn).
[W] Online version contains Web-only data.
[OPEN] Articles can be viewed online without a subscription.
www.plantcell.org/cgi/doi/10.1105/tpc.113.121418

2004). In some cases in vascular plants, isoforms of the enzymes are associated with different subcellular compartments and involved in diverse physiological functions (Chapman and Ohlrogge, 2012). Thus, identifying the genes specifically underlying TAG synthesis is essential for understanding lipid metabolism and for overproducing lipids of commercial interest in microalgae.

Extensive transcriptomic analyses suggested that FA synthesis may be another important regulatory step in TAG production in vascular plants (Bourgis et al., 2011; Troncoso-Ponce et al., 2011; Venglat et al., 2011). Pyruvate and acetyl-CoA, the precursors for FA biosynthesis, are synthesized via multiple metabolic routes. For instance, glycolysis and pentose phosphate pathways are the major contributors for pyruvate production in vascular plants, and a minor amount of pyruvate can also be synthesized from malate by NADP-dependent malic enzyme (Kang and Rawsthorne, 1996; Alonso et al., 2007). Pyruvate is then converted to acetyl-CoA by the pyruvate dehydrogenase complex (PDHC) for de novo FA biosynthesis in the plastid (Lutziger and Oliver, 2000; Lin et al., 2003). In addition, free acetate imported from the mitochondria into the plastid can be converted to acetyl-CoA by an acetyl-CoA synthetase (Roughan and Ohlrogge, 1994). The first step of FA synthesis is catalyzed by acetyl-CoA carboxylase (ACCase) that converts acetyl-CoA to malonyl-CoA, which then serves as a carbon donor for FA chain extension catalyzed by type II FA synthase in the plastid (Ohlrogge and Browse, 1995). A number of key enzymes involved in the production of the precursor for FA synthesis, such as phosphofructokinase, pyruvate kinase (PK), and PDHC, are regulated at the transcript level to increase the carbon fluxes into TAG production in oil palm *Elaeis guineensis* (Bourgis et al., 2011). However, in microalgae, the key enzymes and regulators involved in FA biosynthesis and conversion into TAG and other glycerolipids remain unknown, especially in oleaginous species. Thus, detailed transcriptome and metabolome analyses are essential for reconstructing the metabolic pathways and regulatory networks responsible for TAG synthesis in microalgae.

The nonoleaginous green alga *Chlamydomonas reinhardtii* has served as a model species for investigating the genetic mechanism of TAG production in microalgae because its genome has been sequenced and many specific genetic tools are available (Merchant et al., 2007, 2012; Miller et al., 2010; Boyle et al., 2012). In *C. reinhardtii*, the excess photosynthetically fixed carbons and energy are mainly stored in the form of starch and to a much lesser extent TAG under high light or under high light plus N depletion (Buléon et al., 1997; Li et al., 2010a, 2010b). In oleaginous microalgae (e.g., *Nannochloropsis* spp), TAG is the main carbon and energy reserve along with smaller amounts of the water-soluble polysaccharide chrysolaminarin under stress conditions (Radakovits et al., 2012; Vieler et al., 2012; Wang et al., 2014). The genetic makeup and molecular mechanisms that bestow oleaginous microalgae the ability to produce extraordinary amounts of TAG in response to stress remain to be elucidated.

Nannochloropsis is a genus of unicellular photosynthetic microalgae belonging to the heterokonts and is distributed widely in the marine environment as well as in fresh and brackish waters. *Nannochloropsis* species/strains are of industrial interest due to their ability to grow rapidly, synthesize large amounts of TAGs and high-value polyunsaturated FAs (e.g., eicosapentaenoic acid), and tolerate broad environmental and culture conditions (Sukenik, 1991; Wang et al., 2012). Recently, the genomes of multiple species of *Nannochloropsis* have been sequenced and partially annotated (Radakovits et al., 2012; Vieler et al., 2012; Wei et al., 2013; Wang et al., 2014). Several transcriptomic analyses have also been conducted with *Nannochloropsis* (Vieler et al., 2012; Carpinelli et al., 2013; Zheng et al., 2013); however, the individual-snapshot mRNA analyses, which tested only one or two time points, has failed to capture the temporal dynamics of gene expression. Moreover, the paucity of studies correlating gene expression and metabolite data during oleaginousness has precluded inference and untangling of the causal relationships underlying the complex molecular network involved in lipid metabolism (León-Bañares et al., 2004; Rosenberg et al., 2008).

In this study, we generated large-scale, highly reproducible transcript profiles via mRNA-Seq and lipidome profiles by an electrospray ionization mass spectrometry (ESI/MS) analysis of *Nannochloropsis oceanica* strain IMET1 under N-replete (N+) and N-depleted (N-) conditions. In contrast with the FA analyses adopted by most previous studies on *Nannochloropsis* and many other microalgal species, ESI/MS-based lipidomics analysis directly measured both the end products and the intermediates of glycerolipid metabolism. The congruent global, timely resolved transcriptomic and lipidomic profiles uncovered several key genomic, metabolic, and regulatory characteristics of the oleaginous phenotype of this organism. These findings enhance our understanding of TAG production in microalgae and will assist in the rational genetic engineering of this organism and perhaps of other related species for the overproduction of TAG or other bioproducts.

RESULTS AND DISCUSSION

Global Gene Expression Analysis

To dissect the molecular mechanisms underlying lipid metabolism during oil accumulation, the global gene expression of IMET1 as a function of time (i.e., over six time points, 3, 4, 6, 12, 24, and 48 h) under N+ and N- conditions was measured by mRNA-Seq, with three biological replicates for each sample (Supplemental Table 1). Growth of IMET1 under the two conditions was monitored by optical density measurement (Supplemental Figure 1). The experiment generated 36 high-quality transcript profiles with high reproducibility among the three biological replicates at each time point (Spearman correlation > 0.98; Supplemental Data Set 1). Partitioning around medoids clustering analysis also suggested distinction of the transcriptomes among different time points as well as high reproducibility among the three biological replicates within each time point (Supplemental Figure 2). Furthermore, the time-resolved transcriptomes were validated by quantitative PCR (qPCR) analysis of 13 selected genes over the six time points with the coefficient of determination between qPCR-based and mRNA-Seq–based transcript abundance being 0.9366 (R^2) (Methods; Supplemental Figure 3 and Supplemental Table 2).

A total of 9758 genes, accounting for 97.3% of all of the annotated genes in the IMET1 genome (Wang et al., 2014), were aligned with at least one read (FPKM [fragments per kilobase of

transcript per million mapped reads] value ≥ 1) in each biological sample. Based on the definition of differential gene expression (Methods), 1362 genes (14.0% of total) were found to be significantly upregulated, whereas 1893 genes (19.4% of total) were downregulated in response to N depletion. The upregulated genes were involved in diverse physiological functions without significant functional enrichment. In contrast, the downregulated genes showed functional enrichment, with most of these genes involved in photosynthesis and ribosomal protein synthesis (Supplemental Data Set 2).

The 3255 differentially expressed genes were grouped into 16 clusters based on their temporal expression patterns (Figure 1A). To examine if a given expression pattern was linked to any specific biological functions, the annotated genes in each cluster were manually categorized into 12 functional groups (Supplemental Data Set 2; Figure 1B). The genes with unknown functions accounted for 23 to 64% of the genes in each cluster, representing the largest category; the exception was in cluster C12, where the functional category of protein synthesis, modification, folding, and turnover predominated.

For those clusters predominated by unknown genes, the second largest functional category was designated as the primary functional genes for a given cluster (Figure 1B). In cluster C1, 42% genes encoded components of the photosynthetic apparatuses, such as light-harvesting complex and photosystem reaction center proteins. Transcripts of these genes underwent a sharp decrease in transcript level from 3 to 12 h after the onset of N deprivation, followed by a gradual decrease until 48 h. Cluster C2 was primarily involved in DNA, RNA, and gene expression, including a number of genes encoding enzymes required for DNA replication. The cell cycle category was also enriched in cluster C2. The simultaneous downregulation of DNA replication and cell cycle–related genes after 12 h of N depletion may be attributable to retarded cell division under N deprivation conditions. The primary functional genes of cluster C6 were involved in transport, including the genes encoding ion channels and vesicular trafficking proteins. Most of the genes in this cluster showed progressive upregulation (maximum fold change >20) in response to N deprivation. The primary functional group of cluster C15 is related to protein synthesis, modification, folding, and turnover. Most of the genes in this functional category encoded ribosomal proteins, which were downregulated by ~2-fold. The other clusters were predominantly presented by the category of metabolism, which included genes involved in the biosynthesis and degradation of carbohydrates, amino acids, lipids, and secondary metabolites; these genes exhibited diverse expression patterns (Figure 1B).

Because of the particular interest of this study in lipid metabolism under N-depletion stress, the genes involved in lipid metabolism (e.g., FA metabolism, structural and storage lipid metabolism, and lipid binding/trafficking) in each cluster are listed in Supplemental Data Set 2. A total of 80 differentially expressed lipid metabolism–related genes (DELM) were identified. Regardless of whether the genes were subjected to upregulation, downregulation, or complex regulation, there are several noteworthy features of DELM genes. DELM gene expression patterns are extremely diverse, spreading into all clusters except C12, with the maximum changes in transcript of these genes being <20-fold. DELM genes were particularly enriched in clusters C3, C16, and C10, accounting for nearly 50% of the DELM genes. However, none of these clusters was specialized or enriched with a specific functional group; on the contrary, many genes with the same functions were found in the different clusters. Regulation of the lipid metabolism genes and pathways will be discussed in detail in the corresponding sections below.

Quantitative Analysis of Glycerolipids

In parallel with the global gene expression study, global glycerolipid profiling of IMET1 was performed by an ESI-MS method to characterize the lipid metabolic pathways. Algal samples corresponding to those used in the temporal transcriptomic analysis from the N+ and N- cultures were used for lipidomic analysis. Moreover, considering that changes in molecular species of glycerolipids may lag behind the changes in gene expression in response to nitrogen availability, two more sampling points at 72 and 96 h were added to the lipidomics analysis.

A shotgun mass spectrometry determined nine major glycerolipid classes: monogalactosyldiacylglycerol (MGDG), digalactosyldiacylglycerol (DGDG), sulfoquinovosyldiacylglycerol (SQDG), phosphatidylglycerol (PG), phosphatidylcholine (PC), diacylglyceryl-*O*-4'-(*N*, *N*, *N*,-trimethyl) homoserine (DGTS), phosphatidylinositol (PI), phosphatidylethanolamine (PE), and TAG. Within each of these classes, the acyl groups of individual molecular species were resolved by product ion scanning analysis with optimal collision energy. A total of 55 major molecular lipid species belonging to the nine classes were identified in IMET1 grown under N+ and N- conditions (Supplemental Data Set 3). To achieve lipidome-wide quantitative analysis, algal lipid extracts containing the known amounts of internal standards were separated by two liquid chromatography gradients and detected in the positive and negative mode of ESI/MS, respectively. The cellular contents of the 55 major molecular lipid species over the 96-h period and the total content of the nine classes of glycerolipids (Figure 2) revealed distinct patterns of dynamics in their relative abundances. A small amount of TAG (in the range of 1 to 5 mg g^{-1} cell dry weight) was detected in cells grown under N+ conditions, and it increased by ~3-fold at the end of the lag phase (24 h after inoculation; Figure 2A) and then declined somewhat as cells were dividing (24 to 96 h). After the onset of N depletion, TAG synthesis increased by approximately 400-fold within 96 h. Congruently, the membrane glycerolipids (particularly the photosynthetic membrane lipids like MGDG, DGDG, SQDG, and PG) that dominated under N+ conditions decreased significantly in response to N deprivation. Among the eight classes of membrane glycerolipids, MGDG and PG were most susceptible to N deprivation, with each decreasing by 84% after 96 h under N- conditions.

A heat map showing the fold changes (N-/N+) of all 55 molecular lipid species as a function of time under N- conditions (Figure 3) revealed that 15 major TAG species increased by ~5- to 800-fold at 96 h under N deprivation ($P \leq 0.01$; Supplemental Data Set 3). The TAG species with lower degrees of desaturation, such as TAG 50:2 (16:0/16:0/18:2) and 48:1 (16:0/16:1/16:0), were induced at the early stages of N deprivation (e.g., at 3 and 4 h), while the molecular species of TAG containing polyunsaturated fatty acids (PUFAs), like TAG 52:6 (16:0/16:1/20:5),

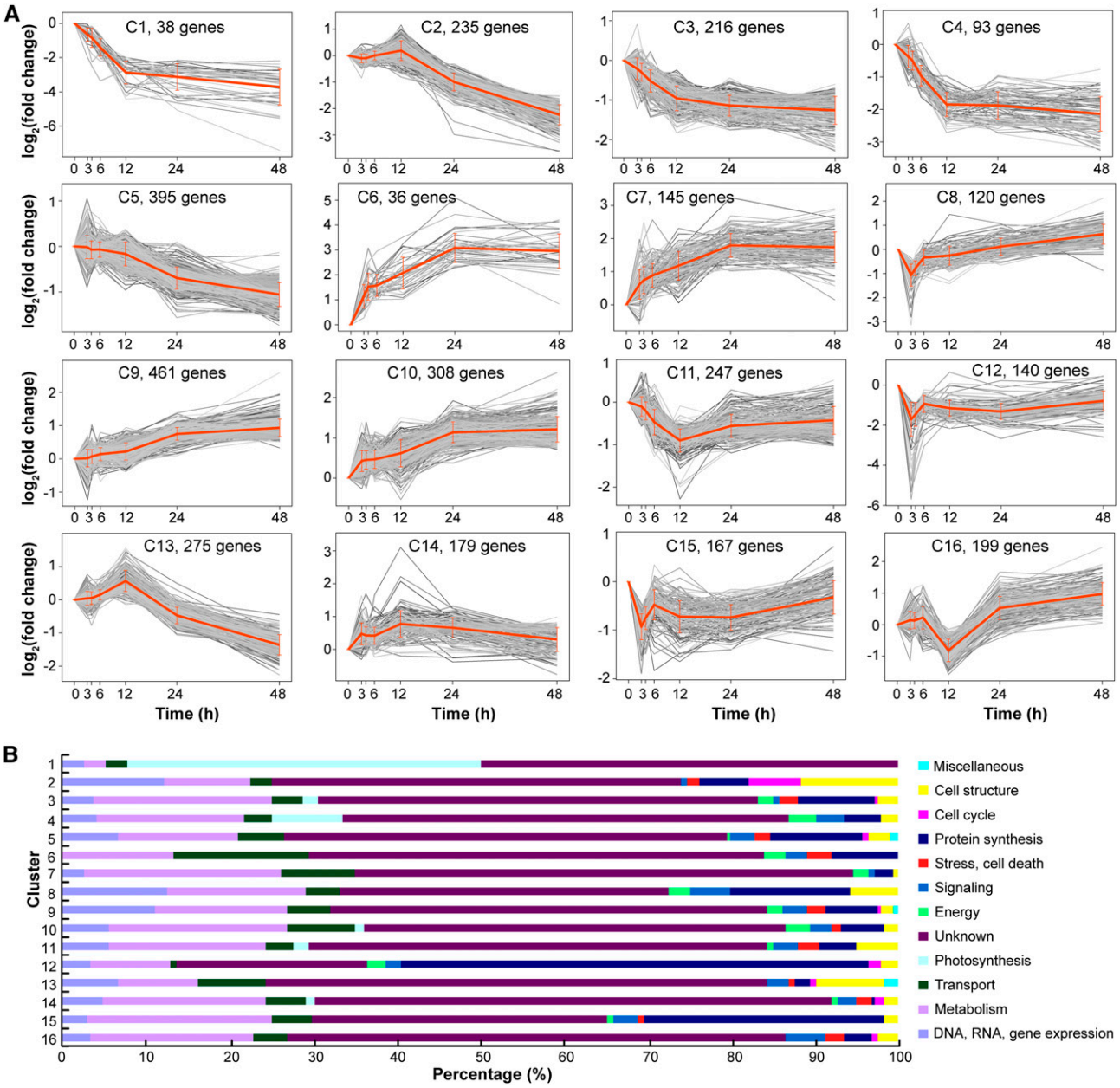

Figure 1. Transcriptional Dynamics and Function of the 3255 Differentially Expressed (N-/N+) Genes.

(A) Expression pattern of the differentially expressed genes grouped into 16 clusters. Mean fold changes [as indicated by $\log_2$(N-/N+)] of genes in a given cluster was plotted as orange lines, with error bars representing the SD (n = 3). The values at time point 0 h were assumed to be zero.
(B) Distribution of genes in manual functional categories within each cluster.

52:5 (16:0/16:0/20:5), and 50:5 (14:0/16:0/20:5), increased considerably after 24 h of N deprivation.

Membrane glycerolipids showed more complex changes than TAG under N- conditions with respect to class and molecular species of lipids. In general, most membrane lipid species decreased in response to N deprivation. In particular, DGTS 32:2 underwent the most rapid reduction at 3 h, followed by DGTS 36:6 and PC 32:2 at 24 h. The degradation of these N-containing molecules can be considered an early response to N deprivation at the molecular lipid species level. After 24 h, a number of photosynthetic membrane lipid species containing PUFAs (e.g., MGDG 34:5 [20:5/14:0], DGDG 34:5 [20:5/14:0], and PG 36:5 [20:5/16:0]), as well as two relatively saturated galactolipid species (MGDG 32:1 and DGDG 32:1), decreased rapidly. By

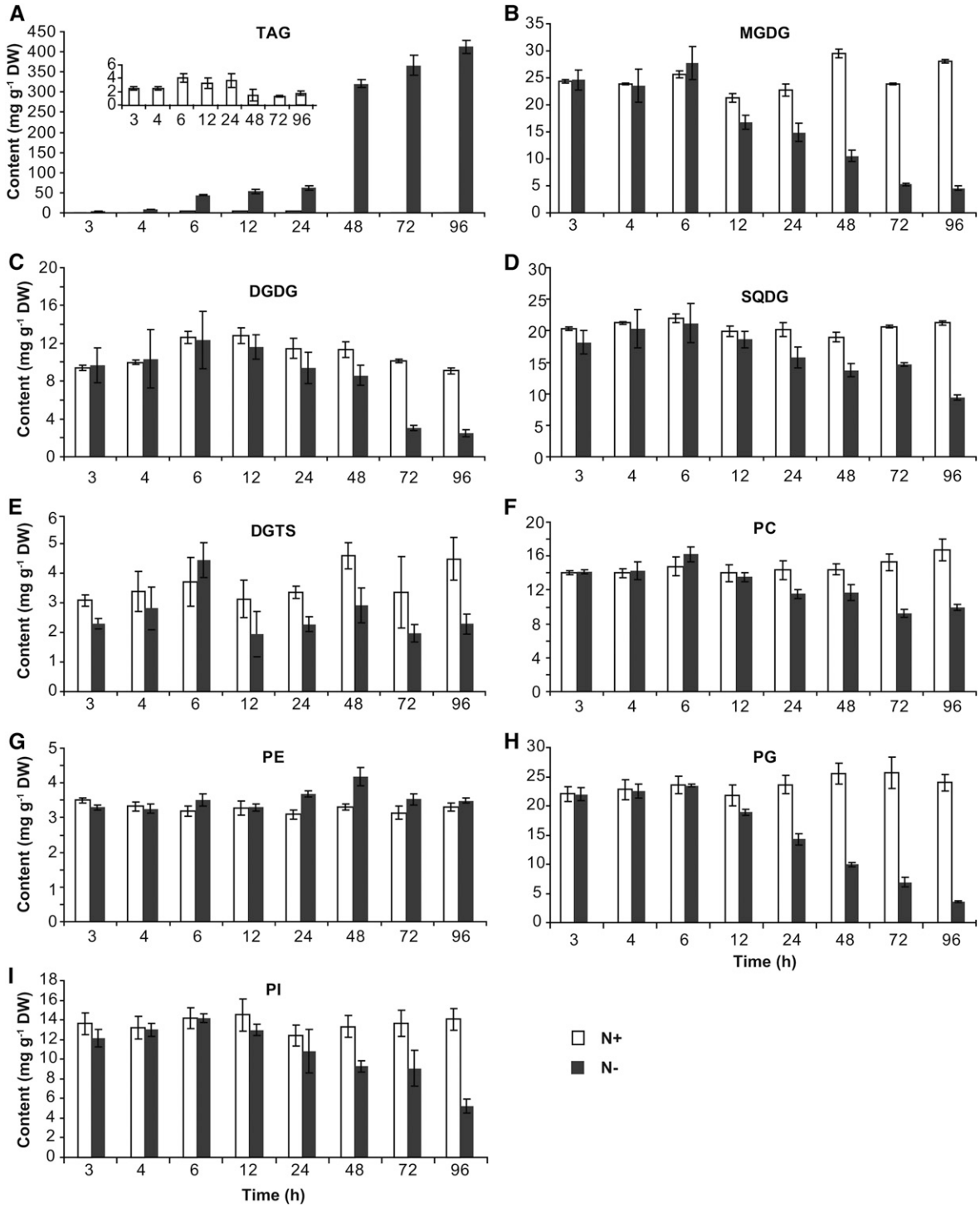

Figure 2. Cellular Content of the Nine Major Glycerolipid Classes in IMET1 as a Function of Time under N+ and N- Conditions.

Values represent means ±SD (n = 3 for **[A]**; n = 4 for **[E]** [DGTS species], and n = 6 for **[B]** to **[I]**). Time refers to the duration (in hours) since the onset of N+ or N- conditions. DW, dry weight.

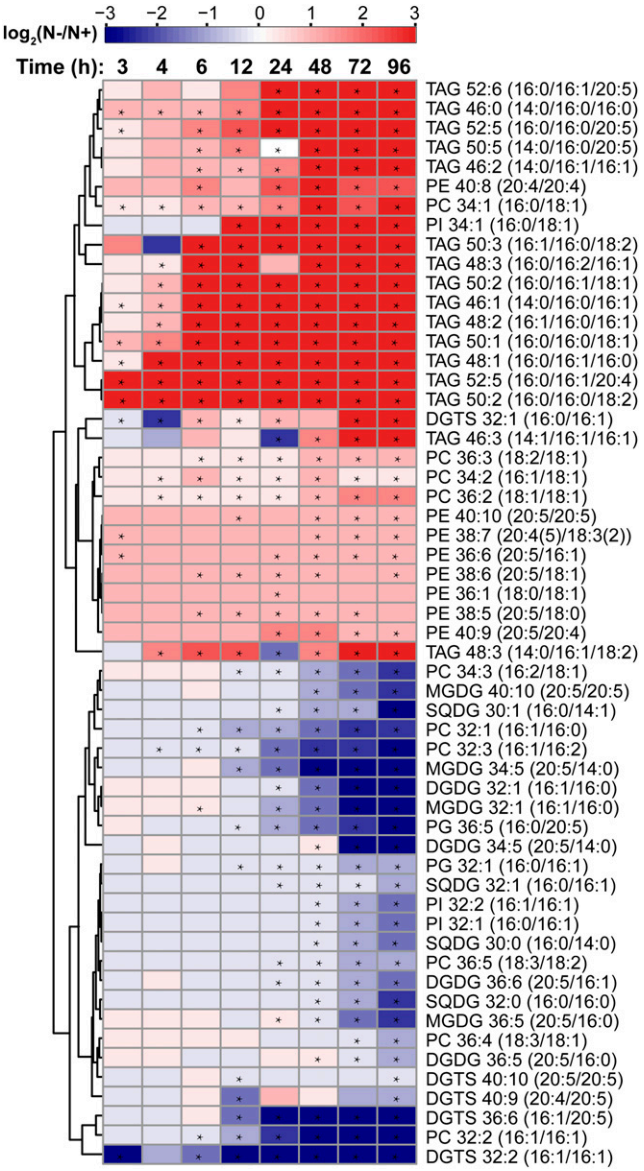

Figure 3. Heat Map Illustrating Variation of the Cellular Content of the Major Molecular Species of Glycerolipids over 96 h under N Deprivation.

Fold change of the lipid content in response to N deprivation was calculated as $\log_2$(lc(Tx, N-)/lc (Tx, N+)) (lc = content of lipid species, Tx = time point, N- = N deprivation, and N+ = N-replete) and displayed in the heat map. Significant differences ($P \leq 0.01$) between N- and N+ are indicated with an asterisk. Acyl chains of glycerolipid species are described by the convention "carbon number: number of double bonds." Values represent means ± SD ($n = 3$ for TAG 48:2 [16:1/16:0/16:1], TAG 48:1 [16:0/16:1/16:0], TAG 50:2 [16:0/16:1/18:1], TAG 50:2 [16:0/16:0/18:2], and TAG 50:1 [16:0/16:0/18:1]; $n = 4$ for DGTS 32:1 [16:0/16:1]; $n = 5$ for DGTS 32:2 [16:1/16:1] and DGTS 40:9 [20:4/20:5]; $n = 6$ [for all other species]). Time refers to the duration (in hours) since the onset of N+ or N- conditions.

contrast, a few PC species (34:1, 34:2, 36:2, and 36:3) increased significantly (by 1.5- to 2.5-fold at 24 h) under N- conditions (Figure 3; Supplemental Data Set 3), indicating the possible presence of PC-based acyl editing in membrane lipid turnover and TAG synthesis. PC acyl editing involves rapid deacylation of PC to release acyl-CoA (Bates et al., 2007, 2009), which is then incorporated into TAG. However, N deprivation did not cause any significant changes in most of the PE species, suggesting that these "housekeeping" lipid species may be involved in maintaining the integrity of cellular membrane structure and function.

TAG Biosynthesis

TAG Synthesis via the Kennedy Pathway

In the IMET1 genome, two DGAT-1 (*DGAT-1A* and *B*) and 11 DGAT-2 genes (*DGAT-2A, B, C, D, E, F, G, H, I, J,* and *K*) were identified (Supplemental Data Set 4), along with one PDAT gene (Wang et al., 2014). The transcriptional dynamics of the 13 DGAT genes were quantitatively determined by mRNA-Seq and confirmed by qPCR (Figure 4; Supplemental Figure 4 and Supplemental Data Set 5). The absolute transcript levels of the 13 DGAT genes were indicated by FPKM values (Figure 4), while the relative transcript level was quantified based on fold changes between the N- and N+ conditions (Figure 5). The 13 DGAT genes showed diverse expression patterns, which were categorized into four groups based upon the effect of N availability on the temporal dynamics of their absolute transcript abundances. *DGAT-2I*, *DGAT-1B*, and *DGAT-2K* were transiently upregulated under N+ conditions with the transcript level peaking at 6, 12, and 24 h, respectively, at levels that were significantly higher than under N- conditions (Figure 4A). Nevertheless, the upregulation of these DGAT genes was concomitant with the increase in TAG from 3 to 24 h under N+ conditions, suggesting that these DGAT genes are responsible for TAG synthesis in the lag and early exponential growth phases of the cells. *DGAT-2F* and *2G* may play a more important role in TAG synthesis under N+ conditions as well, since their transcript levels were higher in N+ than in N- cells. Compared with *DGAT-2I*, *DGAT-1B*, and *DGAT-2K*, the transcript levels of *DGAT-2F* and *2G* peaked at 48 h or at a later time point (Figure 4A), suggesting that these genes may contribute to a greater extent to TAG synthesis in the exponential and stationary growth phases of IMET1 cells.

Seven DGAT genes were upregulated under N- conditions, yet the expression patterns of the individual DGATs were markedly different. *DGAT-2C* and *2D* showed transient upregulation, with their transcript levels peaking at 24 h following the onset of N depletion and declining thereafter (Figure 4B). Rapid upregulation of *DGAT-1A* and *DGAT-2H* occurred at 12 h following the onset of N depletion; *DGAT-2A*, *2B*, and *2E* were similarly upregulated at 24 h. Thereafter, the transcript levels of these DGATs either remained more or less constant (*DGAT-2B*) or continued to increase at a reduced rate (*DGAT-1A*, *DGAT-2A*, *2E*, and *2H*) (Figure 4C). Among these seven DGAT genes, *DGAT-2B* exhibited both the highest absolute level of transcript and the greatest fold change (5.7-fold), falling into C6, a differentially

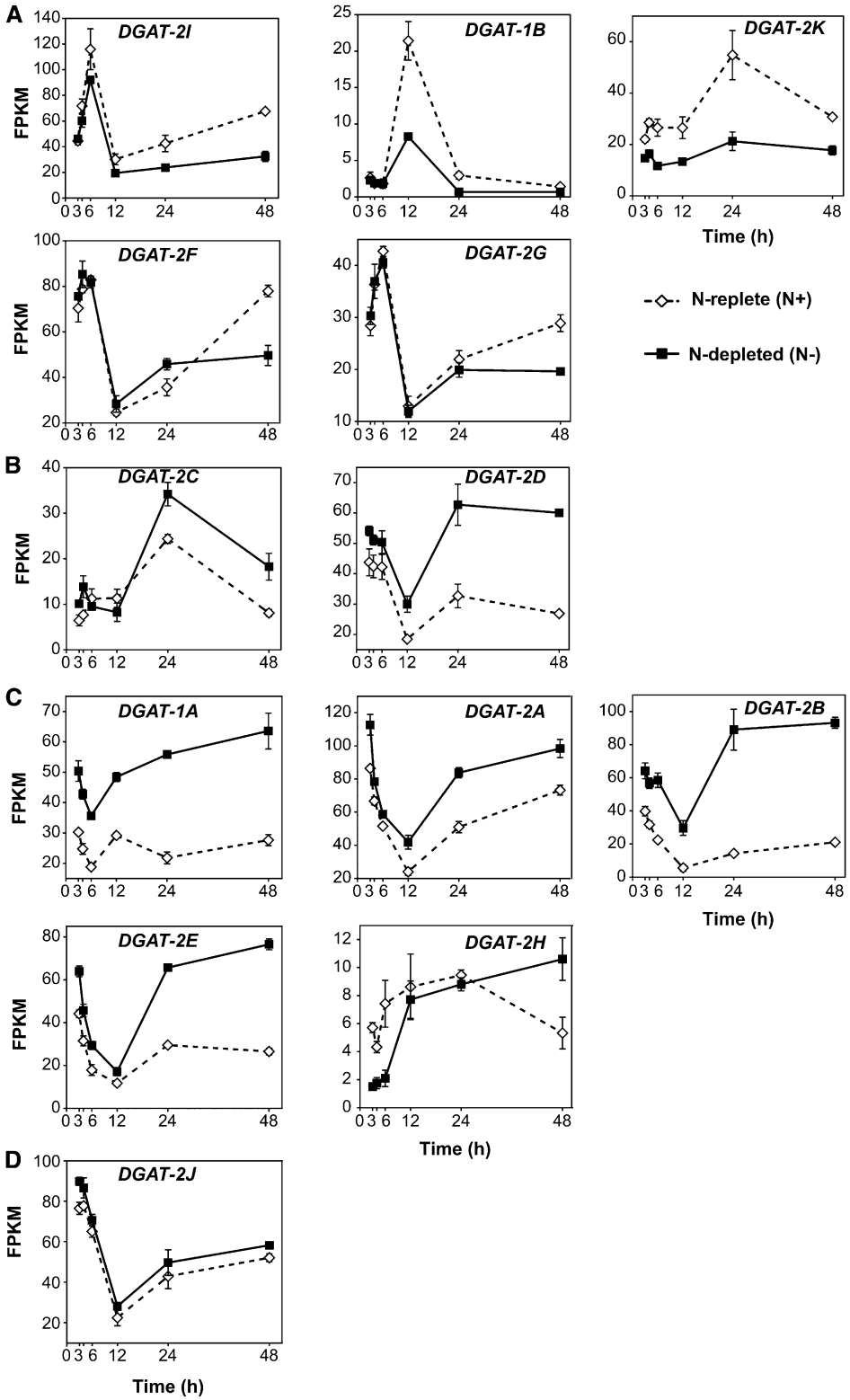

Figure 4. Absolute Transcript Levels (FPKM) of DGAT Genes under N+ and N- Conditions.

Thirteen DGAT genes were classified into four groups based on the transcriptional expression (absolute transcript abundance) patterns of these genes under N-replete and N-depleted conditions. Group **(A)** includes five DGAT genes transiently upregulated under N+ at at least one time point; group **(B)**

expressed gene cluster with the most striking upregulation (Figure 1A), whereas *DGAT-2H* showed the lowest absolute transcript level over the 48-h period. Given that a large number of TAG molecular species increased dramatically after 24 h under N- conditions, the transient or progressive upregulation of these DGATs is likely the major contributor to the bulk of the TAG formed during N depletion. *DGAT-2J* was identified as a "non-N responsive gene," as its transcriptional expression was unaffected by the availability of N in the growth medium (Figure 4D).

Recent studies on *C. reinhardtii* indicate that multiple organelles (e.g., the plastid and endoplasmic reticulum [ER]) are involved in TAG synthesis and assembly (Fan et al., 2011; Goodson et al., 2011; Troncoso-Ponce et al., 2011). To determine possible compartmentalization of TAG synthesis in this organism, SignalP (Petersen et al., 2011), ChloroP (Emanuelsson et al., 1999), Mitoprot (Claros, 1995), and HECTAR (Gschloessl et al., 2008) were used to predict subcellular localization of the 13 DGAT genes. A Type II signal anchor was detected in *DGAT-2A*, *2H*, and *2K* (Supplemental Data Set 6). The Type II signal anchors are signal peptides with an extended N-terminal transmembrane region; thus, the proteins with type II signal anchors are presumed to be located in ER membranes (Gschloessl et al., 2008). These ER-associated DGAT-2 proteins seemed to play differential physiological roles in TAG synthesis under the various environmental conditions: The most abundant ER-associated isoform (encoded by *DGAT-2A*) and a minor isoform (*2H*) were induced under N deprivation (Figures 4C and 5), whereas *2K* was upregulated in the lag and early exponential growth phases under N+ conditions (Figures 4A and 5). In mammalian cells, a subdomain of ER membranes physically associated with mitochondria was found to be enriched in DGAT activity, and a murine DGAT-2 containing a typical mitochondrial transit peptide was present in that specialized subdomain (Stone et al., 2009). A strong signal for mitochondrial transit peptides was detected in DGAT-2I, whose transcriptional pattern strongly suggested a role in TAG synthesis under N+ conditions (Figures 4A and 5).

TAG accumulation in microalgae under stress conditions and in plant leaf cells during senescence may be associated with plastid membrane turnover or degradation (Kaup et al., 2002; Goodson et al., 2011; Troncoso-Ponce et al., 2011), but direct biochemical evidence of DGATs targeting plastids is lacking. For *Nannochloropsis* and other heterokonts derived from secondary endosymbiosis, an ER signal peptide is required in addition to the plastid transit peptide for targeting proteins to the plastid because those plastids are surrounded by a cisterna of ER membrane called the plastid ER (Gibbs, 1979; Gschloessl et al., 2008). In IMET1, the plastid transit peptides were identified in DGAT-1B and 2C proteins (Supplemental Data Set 6), but the ER signal peptide was absent. However, the possible localization of DGAT-1B and 2C in the plastid cannot be ruled out, as the signal peptide may be eliminated due to limitations in gene structure predictions.

The major TAG species of IMET1 were 16:0/16:1/16:0, 16:0/16:0/18:1, 16:0/16:0/18:1, and 16:1/16:0/16:1, with 16:0/16:1/16:0 (48:1) being the most abundant, under either N+ or N- conditions (Supplemental Data Set 3). Given that the FA at the sn-2 position of TAG is determined by the substrate specificity of LPAAT and C16 FA is the preferred substrate of the plastid LPAAT (Lassner et al., 1995; Frentzen, 1998), the major TAG species with C16 FA at the sn-2 position account for more than 80% of total TAG. This suggests that the de novo prokaryotic pathway in the plastid makes the largest contribution to TAG synthesis in this organism. In IMET1, LPAAT is encoded by seven copies of genes in IMET1: Three (g1905, 5355, and 7724) were identified as homologs of *Arabidopsis* plastidic LPAAT1, three (g5448, 5683, and 2077) were closely related to *Arabidopsis* cytoplasmic isoforms LPAAT3, 4, and 5, respectively; and one (g313) had no *Arabidopsis* homologs. Two of the plastid LPAAT genes (g5355 and 7724) were upregulated in response to N deprivation; these are presumably involved in the synthesis of prokaryotic-type TAG molecules under stress conditions (Figure 5).

The first committed step in the Kennedy pathway–mediated TAG synthesis is catalyzed by GPAT. Two putative GPAT genes of IMET1 showed different responses to N deprivation stress. The major isoform g3761, a homolog of *Arabidopsis* plastidic GPAT, was downregulated under N- conditions, whereas g9778, which encodes a homolog of the yeast *Saccharomyces cerevisiae* ER-associated GPAT (SCT1), was slightly upregulated at 48 h after the onset of N deprivation. Similar to the prokaryotic GPAT genes, the transcript level of the single-copy gene encoding a putative plastid PAP (g6690) was reduced under N- conditions. In contrast, four putative cytoplasmic PAP2 genes, including g2171, g4338, g4866, and g9147, were upregulated to different extents during the first 48 h of exposure to N- conditions (Figure 5). It was observed that the expression dynamics of one cytosolic *PAP2* gene (g9147) resembled those of one *LPAAT* gene (g5355) and *DGAT-2D*, all of which were DELM genes that fell into the progressive upregulated cluster C9, whereas another *PAP2* (g4338) was grouped together with *DGAT-2E* in cluster C10, exhibiting a progressive increase at the transcript level as well (Figure 1).

Taken together, the bioinformatics analysis supports the presence of multiple subcellular compartments for TAG synthesis in IMET1. Both the distinct spatial distribution among the various subcellular compartments and the temporally differential expression may result in the large increase in TAG production under N- conditions. Upregulation of the putative eukaryotic Kennedy pathway genes, along with a subset of the prokaryotic Kennedy pathway genes, presumably led to augmented TAG synthesis under N- conditions.

Figure 4. (continued).

includes two DGAT genes with transcript levels peaking at 24 h following the onset of N depletion and declining thereafter; group **(C)** includes five DGAT genes that were progressively upregulated after 12 h under N-; and group **(D)** has a single gene, *DGAT-2J*, that was irresponsive to N availability. Values represent means ± SD (n = 3).

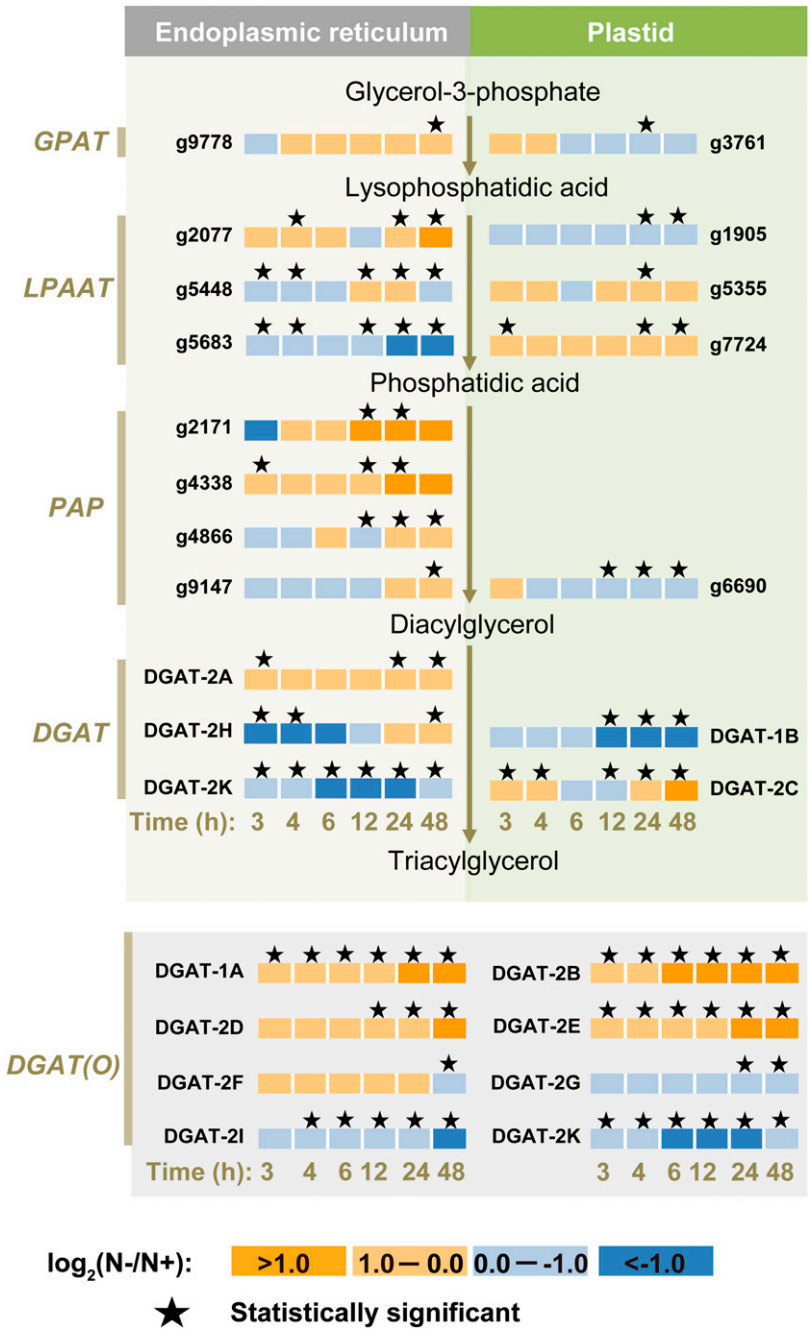

Figure 5. Transcriptional Regulation of the Kennedy Pathway in Response to N Deprivation in IMET1.

Heat map shows the fold changes of transcripts of genes in response to N deprivation. Fold change was calculated as $\log_2$(FPKM(Tx, N-)/FPKM (Tx, N+)) (FPKM = absolute abundance of transcripts, Tx = a time point, N- = N deprivation, and N+ = N-replete). Changes of genes with FDR-corrected P value $\leq$ 0.05 were considered as statistically significant. Time refers to the duration (in hours) since the onset of N+ or N- conditions. Subcellular localizations for GPAT, LPAAT, and PAP were designated based on the experimentally resolved localizations of their eukaryotic homologs. Four putative cytoplasmic PAP2 encoded by g2171, g4338, g4866, and g9147 are shown as ER-associated proteins, given that dephosphorylation of phosphatidic acid in the eukaryotic Kennedy pathway occurs in ER membranes. For DGAT, subcellular localization was predicted using SignalP, ChloroP, Mitoprot, and HECTAR. DGAT presumably targeted to organelles other than plastid and ER is shown in the box labeled *DGAT(O)*.

Recycling of FA from Membrane Glycerolipids for TAG Biosynthesis

Recycling of existing FA from membrane glycerolipids has been demonstrated to contribute to TAG in *C. reinhardtii* (Li et al., 2012; Yoon et al., 2012). This process can be catalyzed by PDAT, a multifunctional enzyme exhibiting phospholipid/galactolipid: DAG acyltransferase, DAG:DAG transacylase, and lipase activities with broad substrate specificity (Yoon et al., 2012). It has been suggested that PDAT is mainly involved in TAG synthesis under N+ conditions, as well as at the early phase of N deprivation in *C. reinhardtii*. A single-copy *PDAT* of IMET1 was slightly upregulated by ~50% at 48 h in response to N deprivation (Supplemental Data Set 5), suggesting that the PDAT-mediated conversion of membrane lipids into TAG occurred under N+ conditions and was enhanced under N- conditions.

In addition to PDAT, a number of lipase genes with the putative function of recycling FA from membrane lipids for TAG synthesis in *C. reinhardtii* were found to be greatly elevated under N- conditions (Miller et al., 2010). Among them, a galactolipase gene designated as *PSD1* has been found to be involved in the turnover of MGDG and TAG in *C. reinhardtii* (Li et al., 2012). In IMET1, PDAT seemed to play a minor role in TAG synthesis under N- conditions, as it was only slightly elevated at the transcript level. By contrast, a homolog of *PSD1* was upregulated by ~3-fold at 24 h following N deprivation and remained constant thereafter. This was coincident with the degradation of MGDG in IMET1, suggesting that lipase-mediated membrane degradation is likely the major contributor to the channeling of FA from photosynthetic membranes to TAG under N- conditions. In IMET1, 37 putative lipases genes were identified, 14 of which exhibited upregulation to various extents under N deprivation (Supplemental Data Set 5). Among the upregulated lipase genes, g7236 exhibited the greatest fold-change (>4-fold upregulation; found in cluster C7; Figure 1A).

The upregulated lipases, especially those predicted to be galactolipases, may be involved in TAG production, given that galactolipids are the most abundant membrane lipids in IMET1 and are largely degraded under N deprivation. In vascular plants, most of the known galactolipases belong to the patatin family, which hydrolyzes galactolipids to release free FA under various biotic and abiotic stress conditions (Matos et al., 2000, 2001; Yang et al., 2007). In IMET1, three of the seven putative patatin genes (g9879, g2582, and g3354) were upregulated under N deprivation.

The occurrence of membrane lipid–derived PUFAs in the TAG pool is considered to be additional evidence supporting our hypothesis that FA can be recycled for TAG synthesis under stress (Simionato et al., 2013). In IMET1, EPA occurs in several classes of membrane glycerolipids, such as MGDG, DGDG, and PG, under N+ conditions (Figure 3). Most of these EPA-containing membrane lipid species decreased by approximately 20 to 50% ($P < 0.01$; Supplemental Data Set 3) after 24 h under N- conditions, with a concomitant increase of EPA-containing TAG species, suggesting that TAG synthesis under N- conditions used the FA cleaved from EPA-containing membrane lipids. However, the amount of EPA in the TAG pool is far less than that measured in the membrane glycerolipids. For example, the total content of EPA in EPA-containing TAG was 16.4 μmol g^{-1} dry weight under N depletion at 96 h, whereas the decreased amount of membrane glycerolipid-associated EPA at the same time point was approximately 67 μmol g^{-1} dry weight (Supplemental Data Set 3). This discrepancy indicated that only a small portion of EPA cleaved from membrane glycerolipids was used for TAG synthesis.

Sources of Carbon Precursors for Glycerolipid Synthesis

FA Synthesis and Transport

Two multifunctional monomeric ACCase genes were identified in the IMET1 genome. One *ACCase* (g4840) putatively encodes a plastid-targeting protein, while the other (g8944) encodes a cytosolic isoform. The transcript level of g4840 decreased ~2-fold at 12 h and then recovered to 80% of the basal level under N+ conditions, while g8944 was downregulated immediately after the onset of N deprivation and decreased ~3-fold at 48 h (Supplemental Data Set 5). Given that the ACCase genes were considerably downregulated while the total glycerolipid content increased 5-fold following N deprivation, we speculated that *ACCase* was present in excess in terms of transcript or enzyme quantity for FA biosynthesis in IMET1 under both N+ and N- conditions. This explains why previous attempts to increase lipid content in microalgae and plants by overexpressing ACCase had limited success (Dunahay et al., 1995; Roesler et al., 1997). Malonyl-CoA, the product of ACCase, is transferred from CoA to an acyl carrier protein (ACP) by a malonyl-CoA:acyl protein malonyltransferase (MCMT) to form malonyl-ACP, which then enters into a series of condensation reactions to form 16- or 18-carbon FA. A single-copy ACP gene increased its transcripts by ~2-fold at 48 h under N- conditions, whereas *MCMT* was downregulated in response to N deprivation.

The extension of FA from malonyl-ACP in the plastid is iteratively catalyzed by a type II fatty acid synthase system consisting of 3-ketoacyl-ACP synthase (KAS), 3-ketoacyl-ACP reductase (KAR), hydroxyacyl-ACP dehydrogenase (HAD), and enoyl-ACP reductase (ENR) (Ohlrogge and Browse, 1995). In IMET1, six *KAS*, three *KAR*, one *HAD*, and three *ENR* genes were identified (Supplemental Data Set 5). In vascular plants, condensation of acetyl-CoA with acyl-ACP is catalyzed by three different types of KAS: The first condensation reaction of acetyl-CoA and malonyl-ACP is catalyzed by KAS III; subsequent condensation reactions up to the formation of C:16:0-ACP are catalyzed by KAS I; and the final condensation reaction to produce C18:0-ACP requires KASII (Li-Beisson et al., 2010). In IMET1, a single-copy KAS III gene (g4061) showed an ~2-fold decrease at 24 h, followed by an ~4-fold decrease at 48 h. The single-copy KAS I gene (g1093) showed transient upregulation (~20%) at 3 h following N deprivation but decreased ~2-fold at 48 h. Two putative KAS II genes (g4062 and g8736), a single-copy HAD gene (g2692), and the major isoform ENR gene (g5253) were downregulated ~1.5- to 2-fold. Therefore, similar to the downregulation of ACCase, the transcriptional expression of the plastid type II fatty acid synthase system was globally suppressed under N- conditions. Given that the KAS encoded by g9573, which was upregulated ~2-fold at the transcript level after 24 h, shares 49.2% sequence similarity

with the mitochondrial KAS of *Arabidopsis* (At2g04540) (Yasuno et al., 2004), we propose that mitochondria serve as an additional site for the synthesis of bulk FA in IMET1, as in vascular plants (Gueguen et al., 2000; Wada et al., 1997), particularly under N- conditions. The other components of the mitochondrial FAS system have not yet been identified in the IMET1 genome.

FA synthesis in the plastid is terminated either by plastidic acyltransferases (e.g., plastid GPAT or LPAAT) for direct glycerolipid assembly or by an acyl-ACP thioesterase (TE) that cleaves FA from acyl-ACP (Joyard et al., 2010). Among the three *TE* genes identified in IMET1, the transcript level of one (g9763) increased 2.7-fold at 24 h and 3.1-fold at 48 h under N deprivation (Supplemental Data Set 5). We speculated that the TE encoded by this gene may preferentially release C16:0 from acyl-ACP, ultimately contributing to the accumulation of C16:0-containing TAG. The released FA in the plastid is subsequently converted to acyl-CoA by long-chain acyl-CoA synthetases (LC-FACS) in the plastid envelopes of *Arabidopsis* (Fulda et al., 2002; Zhao et al., 2010). In IMET1, five of the 11 putative LC-FACS genes were upregulated in response to N deprivation, among which g5786, g8758, and g9817 showed significant increases in mRNA at least at one time point, and g6018 and g9361 displayed gradual increases in transcript level over 48 h. In contrast, the transcript level of all other isoforms of LC-FACS was reduced to various extents. The different transcriptional expression patterns of these LC-FACS isoforms may reflect their different subcellular localizations, distinct substrate specificities, or varied timings for expression. The resulting acyl-CoA molecules are then transferred with the aid of cytosolic acyl-CoA binding proteins (ACBP) to the ER (Koo et al., 2004). Four ACBP genes (i.e., g2168, g5924, g2727, and g7235; Supplemental Data Set 5) were identified in IMET1: Two (g2727 and g7235) were elevated at the transcript level over 48 h, whereas g5924 was downregulated progressively following N deprivation; g2168 was almost undetectable under both N+ and N- conditions. The encoded ACBP proteins may work in concert to serve as intracellular acyl-CoA transporters that maintain an appropriate cytosolic acyl-CoA pool.

The common end products of de novo FA biosynthesis are C16:0, C18:0, and C18:1 in the plastids of algae and vascular plants (Ohlrogge and Browse, 1995; Li-Beisson et al., 2010). To synthesize glycerolipids of various chain lengths with different unsaturation levels, a series of elongation and desaturation reactions are required. In vascular plants, stearoyl-ACP desaturase (Δ9-desaturase) is the only soluble enzyme that introduces a double bond to the Δ9 position of C18:0-ACP to form C18:1-ACP, whereas other desaturases are membrane proteins that desaturate the acyl-groups of lipid molecules (Browse et al., 1989, 1985; Iba et al., 1993; Heilmann et al., 2004; Kachroo et al., 2007; Gao et al., 2009). In plastids, the Δ9-desaturase–catalyzed desaturation reaction uses reduced ferredoxin as the electron donor and molecular oxygen as one of the substrates (Schultz et al., 2000). In IMET1, the transcript level of one putative soluble Δ9-desaturase (g481) increased immediately upon the onset of N deprivation and remained at a high level (Supplemental Data Set 5). The transcriptional upregulation of this gene was consistent with the drastically increased cellular content of C18:1 under N- conditions in this organism (Xiao et al., 2013). The upregulation of the Δ9-desaturase reflected its physiological role in the stress response, which is presumably involved in oxidizing photosynthetically generated ferredoxin with the concomitant reduction of molecular oxygen into water, thus relaxing the overreduced photosynthetic electron transport to prevent the formation of excess reactive oxygen species. It is noteworthy that the single Δ9-desaturase gene g481 was co-upregulated with two ACBP genes (g2727 and g7235), one LC-FACS gene (g5786), and the putative mitochondrial KAS gene (g9573), all of which belong to cluster C10 (exhibiting an expression pattern of progressive upregulation; Figure 1A); this is an example of the coupling of the synthesis and transport of FAs with the relaxing of the photosynthetic electron transport chain as a molecular or physiological protective mechanism, among other functions, to cope with photooxidative stress.

Photosynthetic Carbon Precursors and Partitioning

Glyceraldehyde-3-phosphate (G3P), a key product of the Calvin cycle, is converted to pyruvate, the precursor for FA biosynthesis, via glycolysis pathways (Figure 6). In vascular plants, glycolysis occurs in plastids and the cytosol, which produces pyruvate from glucose while generating the high-energy compounds ATP and NADH (Plaxton, 1996). All the components of the glycolysis pathway were identified in IMET1, and subcellular localization analysis of these components revealed that the plastid only possesses the lower part of the glycolysis pathway (from G3P to pyruvate) along with a plastidic fructose-1,6-bisphosphate aldolase (ALDO) that converts fructose 1,6-biphosphate (F1,6P) to G3P (Supplemental Data Sets 5 and 6; Figure 6). All of the putative plastid glycolytic genes except for the PK encoded by g8432 were downregulated at the transcript level in response to N deprivation. The plastid PK gene (g8432) is the most abundant of the four putative PK genes and was progressively upregulated during the first 48 h of exposure to N- conditions (Figure 6).

In addition to the partial glycolysis pathway in the plastid, a complete cytosolic glycolysis pathway was identified by subcellular localization prediction. All genes involved in the conversion of G3P to pyruvate were significantly upregulated following N deprivation. Although the cytosolic glycolysis pathway was upregulated, the absolute transcript level of the plastid glycolytic genes was higher than their cytosolic counterparts, suggesting that the plastid glycolysis pathway generates the bulk of pyruvate under both N+ and N- conditions, whereas the cytosolic glycolysis pathway is accelerated specifically under stress.

The gene clustering analysis based on expression patterns revealed that a number of glycolytic genes were temporally coregulated at the transcript level (Pearson's correlation; $P < 0.05$; Supplemental Data Set 5). For instance, three of the eight plastid glycolytic genes, including one encoding aldolase (*ALDO*, g1829), one glyceraldehyde-3-phosphate dehydrogenase (*GPDH*, g10357), and one phosphoglycerate kinase (*PGK*, g8651), were grouped into cluster C4, exhibiting a sharp decrease in transcript during the first 12 h under N- conditions (Figure 1A). On the other hand, three putative cytosolic glycolytic genes, including one phosphofructose kinase (*PFK*, g8588), one phosphoglycerate mutase

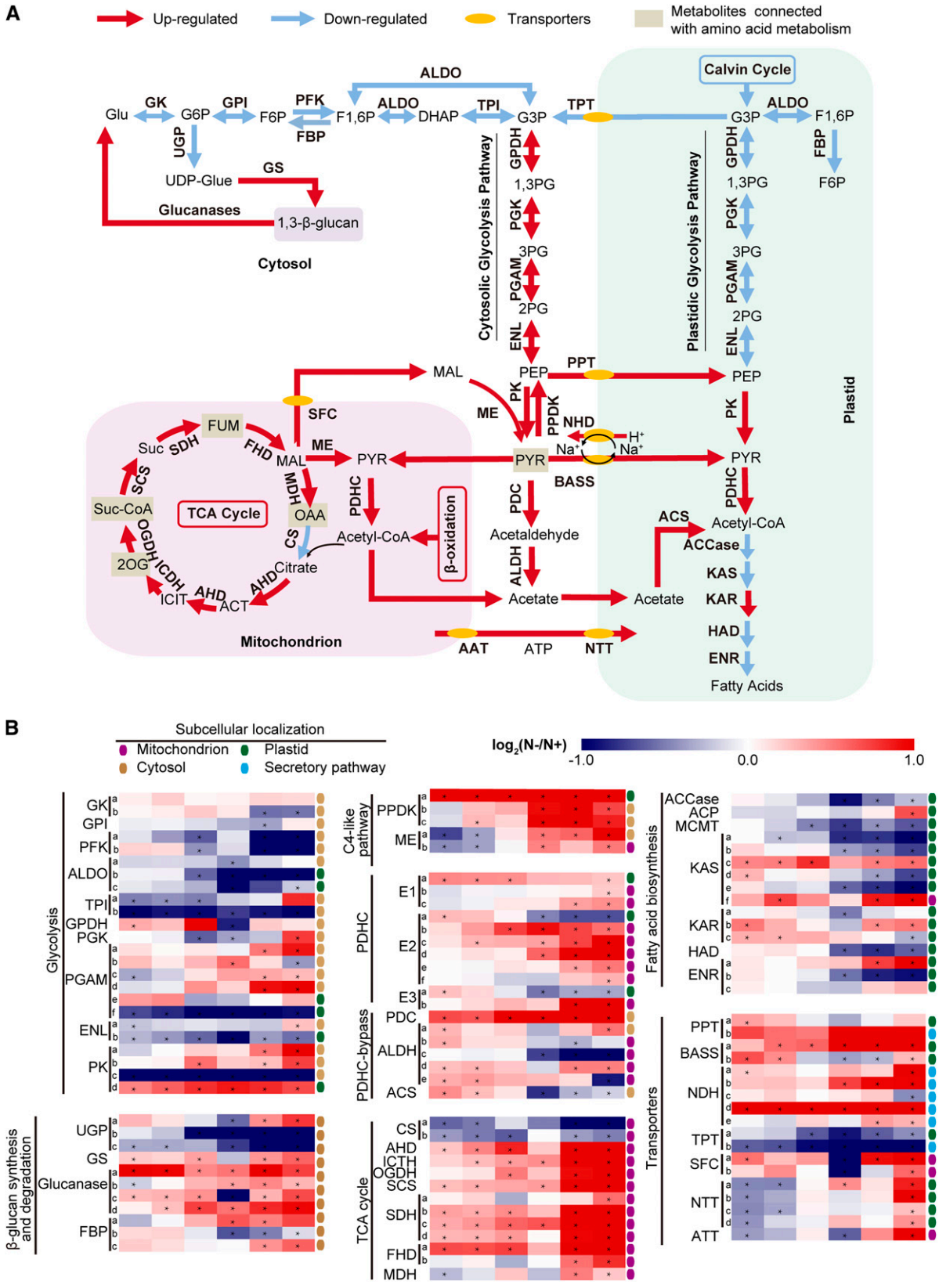

Figure 6. Transcriptional Regulation of Central Carbon Metabolism in Response to N Deprivation in IMET1.

(*PGAM*, g10298), and one *PK* (g6372), were grouped into cluster C9, which consists of a number of genes moderately up-regulated during the first 48 h of exposure to N- conditions.

The remarkable increase in glycerolipids can result from not only the accelerated partitioning of newly photosynthetically fixed carbon through glycolysis but also from the recycling of carbon fluxes derived from the degradation of existing macromolecules (e.g., carbohydrates and proteins) into the precursors for lipid biosynthesis. Previous studies of the unicellular green alga *C. reinhardtii* suggested that conversion of storage polysaccharides (e.g., starch) into the precursors for lipid biosynthesis contributed to TAG accumulation under N- conditions (Li et al., 2010b, 2011; Work et al., 2010). Microscope observations indicated *Nannochloropsis* cells lack pyrenoid starch (Vieler et al., 2012; Dong et al., 2013), consistent with the absence of genes responsible for starch biosynthesis in the IMET1 genome. Laminarin and chrysolaminarin, which are glucans with various ratios of β-(1,3) to β-(1,6)–linked Glc, with predominantly β-(1,3)-linkages, have been suggested to be the major storage carbohydrate in heterokonts (Beattie et al., 1961). The synthesis of storage glucan in heterokonts has not been elucidated at the molecular level, but biochemical analysis indicated that a UDP-glucose pyrophosphorylase (UGPase) and a β-1,3-glucan synthase were responsible for the production of chrysolaminarin in diatoms (Roessler, 1987, 1988). Among the three UGPase genes (g447, g637, and g2034) identified in IMET1, g447 was upregulated ~1.5- to 2-fold after 24 h of N deprivation, whereas g637 and g2034 were substantially suppressed under N deprivation (Figure 6). Considering that the absolute transcript level of g637 and g2034 was higher than that of g447, the overall transcript level of UGPase was reduced by ~70% at 48 h. A single-copy β-1,3-glucan synthase gene was identified, and its absolute transcript level slightly increased under N deprivation relative to N+ conditions. Conversely, a number of genes involved in β-1,3-glucan degradation, including a putative endoglucanase gene (g5401), an endo-1,3-β-glucosidase gene (g1660), a glucan 1,3-β-glucosidase (g4700), and an exo-1,3-β-glucosidase gene (g7570), were upregulated 1.3- to ~2-fold during the first 48 h of exposure to N deprivation. The degradation product Glc can be converted into pyruvate via the cytosolic glycolysis pathway (Figure 6). Thus, the upregulation of the genes involved in laminaran/chrysolaminaran degradation may represent an additional mechanism by which photosynthetically fixed carbon is diverged into FA and TAG synthesis, particularly under N depletion.

Multiple Routes for Acetyl-CoA Synthesis in IMET1

The formation of acetyl-CoA from the substrate pyruvate in the plastid for FA biosynthesis is believed to be mainly catalyzed by a PDHC (Oliver et al., 2009) that bridges the glycolysis and lipid biosynthesis pathways. PDHC consists of three subunits: E1, E2, and E3. Both the plastidial and mitochondrial type PDHC genes were identified in IMET1 (Supplemental Data Set 6), and the transcript levels of the plastidial E1 (g4805), E2 (g946), and E3 (g163) were 2- to ~6-fold higher than those of the putative mitochondrial PDHC genes (Figure 6), suggesting that the plastid is the major site of acetyl-CoA formation. All the subunits of the plastidial PDHC were slightly upregulated at 3 h, whereas the mitochondrial PDHC genes did not increase in transcript level until 24 to 48 h of exposure to N deprivation.

Acetyl-CoA can also be produced from pyruvate via a so-called "PDHC bypass," in which pyruvate is converted to acetate by a pyruvate decarboxylase (PDC) and an aldehyde dehydrogenase (ALDH) (Figure 6). A single-copy PDC gene that may encode a cytosolic protein was found in IMET1 and its transcripts increased 6-fold during 48 h of exposure to N deprivation. Five copies of ALDH genes were found in IMET1, four of which increased in transcript under N deprivation. One ALDH (g7934) was annotated as a cytosolic enzyme; the others may reside in the mitochondria, as they all possess a strong mitochondrial transit peptide signal (Supplemental Data Set 6). It is likely that cytosolic PDC and ALDH convert the pyruvate produced via the cytosolic glycolysis pathway into acetate. The acetate produced by PDHC bypass in the cytosol, along with the acetate exported from the mitochondria, is then activated to acetyl-CoA by the plastidic acetyl-CoA synthetase. In IMET1, two copies of the acetyl-CoA synthetase genes were

Figure 6. (continued).

(A) Transcriptional regulation of central carbon metabolic pathways related to TAG biosynthesis. Transcriptional regulation of genes is indicated by blue (downregulated) and red (upregulated) arrows, respectively.

(B) A heat map illustrating the transcriptional dynamics of individual genes in the central carbon metabolic pathways in response to N availability. Fold change was calculated as $\log_2$(FPKM(Tx, N-)/FPKM (Tx, N+)) (FPKM = absolute abundance of transcripts, Tx = a time point, N- = N deprivation, and N+ = N-replete). For proteins encoded by multiple copies of genes, the changes in total transcripts of the isogenes were used to determine the regulation pattern. Statistical analysis was conducted between the two gene expression data sets (N- and N+) at a given time point. Significant changes (FDR-corrected P value ≤ 0.05) are indicated as asterisks in the heat map.

1,3PG, 1,3-biphosphoglycerate; 2OG, α-ketoglutarate; 2PG, 2-phosphoglycerate; 3PG, 3-phosphoglycerate; AAT, ADP/ATP transporter; ACS, acetyl-CoA synthetase; ACT, aconitate; AHD, aconitate hydratase; ALDO, fructose-1,6-bisphosphate aldolase; CS, ATP citrate synthase; DHAP, dihydroxyacetone phosphate; ENL, enolase; ENR, enoyl-ACP reductase; F1,6P, fructose 1,6-biphosphate; FBP, fructose bisphosphatase; F6P, fructose-6-phosphate; FHD, fumarate hydratase; FUM, fumarate; G6P, glucose-6-phosphate; GK, glucose kinase; Glu, glucose; GPDH, glyceraldehyde-3-phosphate dehydrogenase; GPI, glucose phosphate isomerase; GS, 1,3-β-glucan synthase; HAD, hydroxyacyl-ACP dehydrogenase; ICDH, isocitrate dehydrogenase; ICIT, isocitrate; MHD, malate dehydrogenase; NTT, nucleotide transporter; OGDH, 2-oxoglutarate dehydrogenase; PGAM, phosphoglycerate mutase; PGK, phosphoglycerate kinase; PFK, phosphofructose kinase; PPDK, phosphate dikinase; PPT, Pi/PEP translocator; PYR, pyruvate; SCS, succinyl-CoA synthetase; SDH, succinate dehydrogenase; SUC, succinyl-CoA; TPI, triosephosphate isomerase; SFC, succinate/fumarate carrier. Transcripts of all the genes are listed in Supplemental Data Set 5.

present. One (g1733) had a high basal transcript level and underwent a slight increase in transcript level after 3 to 4 h of exposure to N deprivation, whereas the other (g3155) had a low basal transcript level and displayed a 3-fold increase over 48 h under N- conditions (Supplemental Data Set 5).

Role of Mitochondria in Lipid Metabolism

Mitochondria have been suggested to play multiple roles in TAG synthesis in vascular plants, including providing precursors for FA elongation in the cytosol and for de novo FA biosynthesis in the plastid (Ohlrogge and Browse, 1995; Schwender et al., 2006). In this study, DGAT-2I and one putative KAS (encoded by g9573) were predicted to be localized in the mitochondria. Their transcriptional patterns indicate that TAG and FA synthesis reactions may occur in the mitochondria and may be stimulated under N deprivation in IMET1. Moreover, it is speculated that the mitochondria may contribute to TAG synthesis in IMET1 by recycling carbon skeletons from degraded membrane glycerolipids via FA β-oxidation. To test this hypothesis, all candidate genes involved in β-oxidation from the IMET1 genome were identified and their temporal transcriptional patterns were compared (Supplemental Data Set 5). Because the β-oxidation pathway occurs in mitochondria and peroxisomes in vascular plants (Gerhardt, 1992; Masterson and Wood, 2001), the putative proteins were analyzed by Mitoprot and PlantPTS1 to predict the mitochondrial transit peptide or peroxisomal signal peptide (Supplemental Data Set 6). In IMET1, two acyl-CoA dehydrogenase genes (g1094 and g3725), which catalyze the initial step of FA β-oxidation in mitochondria (Kunau et al., 1995), were significantly upregulated from 4 to 48 h following N deprivation. Several other components associated with mitochondrial β-oxidation, including one gene (g1681) encoding 3-ketoacyl-CoA thiolase, four genes (g28, g1300, g4575, and g9197) encoding enoyl-CoA hydratase, and one 3-hydroxyacyl-CoA dehydrogenase gene (g8580), were concomitantly upregulated in response to N deprivation (Supplemental Data Set 5).

Acetyl-CoA produced from FA β-oxidation can either be broken down into CO_2 via the tricarboxylic acid (TCA) cycle to produce NADH that fuels ATP synthesis by oxidative phosphorylation in the mitochondria, or it can be converted into carboxylic acids via noncyclic TCA reactions for a variety of biosynthetic processes (Sweetlove et al., 2010). Under N- conditions, transcripts of all enzymes in the TCA cycle except citrate synthase were upregulated (>2-fold) (Figure 6). It is noteworthy that the most remarkable increase (>4-fold) in transcript among those TCA genes was found in one of the fumarate hydratase genes (g750) for the synthesis of malate, which can be subsequently exported to the cytosol for the production of pyruvate by a NAD(P)-malic enzyme (ME). Taken together, these clues suggest that the production of malate and/or oxaloacetate is accelerated through the TCA reactions under N- conditions. Moreover, the intermediates of the TCA cycle (e.g., 2-oxoglutarate, succinyl CoA, fumarate, and oxaloacetate) are linked to amino acid metabolism. N deprivation–triggered protein and amino acid degradation can increase the carbon flux into these TCA cycle intermediates (Hockin et al., 2012). Therefore, the upregulation of the TCA reactions, coupled with the elevation of FA β-oxidation in mitochondria, may pinpoint an enhanced recycling of carbon skeletons from degraded membrane lipids and proteins for TAG synthesis.

Transport of Metabolites and Energy for FA Synthesis in the Plastid

Transcriptomic analysis revealed a number of N deprivation–induced genes encoding transporters that may direct carbon precursors and energy to FA biosynthesis in the plastid. Two genes (g2277 and g9518) encoding a putative bile acid:Na^+ symporter (BASS), which mediates sodium-coupled pyruvate import into plastids (Furumoto et al., 2011), gradually increased in transcript level following N deprivation. In this pathway, the balance of coupled-sodium influx is maintained by a sodium:proton antiporter (NHD). Nine *NHD* isoforms were identified in IMET1, and the transcript levels of six of these (g7561, g9360, g4014, g2617, g10029, and g5328) were upregulated under N deprivation (Figure 6; Supplemental Data Set 5). Interestingly, one putative *NHD* gene (g9360) clustered with one *BASS* gene (g2277) in cluster C10, indicative of their transcriptional co-upregulation (Pearson's product moment correlation coefficient 0.94; $P < 0.05$). A putative phosphate/phosphoenolpyruvate translocator encoded by g6871 was induced immediately after the onset of N deprivation, and its transcript level increased 3-fold after 24 h of exposure to N deprivation. In *Arabidopsis thaliana*, phosphate/phosphoenolpyruvate translocator imports cytosolic phosphoenolpyruvate (PEP) into the plastid stroma in exchange for Pi (Fischer et al., 1997). PEP can be converted into pyruvate and then acetyl-CoA for FA synthesis in the plastid (Rawsthorne, 2002). Simultaneously, the export of PEP from the plastid into the cytosol was inhibited, as indicated by down-regulation of three genes encoding triose-phosphate/phosphate translocator (TPT) isoforms, which are responsible for exporting photosynthetically fixed carbon (e.g., triose phosphates and 3-phosphoglycerate) out of the plastids in *Arabidopsis* (Weber and Linka, 2011). The transcript level of the first TPT gene (g521) was reduced to 65% of the N+ after 3 h under N depletion and to 22% after 12 h under N depletion. The second one (g1018) decreased to 54% of the N+ after 12 h of exposure to N- conditions, while the third one (g6303) was moderately reduced.

Several lines of evidence suggested that IMET1 cells may be able to boost ATP production in mitochondria and probably also in the cytosol and then export it into the plastid to meet the energy demands for FA biosynthesis, particularly when photosynthesis-based ATP production is considerably decreased under N deprivation (Figure 6): (1) The transcript level of a mitochondrial ATP/ADP translocator (g4664) involved in exporting ATP from mitochondria to the cytosol was slightly reduced at 3 h and then increased gradually to a maximal value at 48 h following N deprivation; and (2) ATP import from the cytosol into plastids may be catalyzed by a plastidial nucleotide transporter in vascular plants (Flügge et al., 2011). In IMET1, four putative nucleotide transporter genes (g1797, g1694, g4356, and g4016) were annotated as plastidic ATP/ADP transporter genes, all of which were moderately upregulated at 48 h in response to N deprivation (Supplemental Data Set 5). Additionally, a number of genes encoding the mitochondrial transporters for exporting

organic acids (e.g., malate and citrate) were upregulated (Figure 6). For instance, the export of malate from mitochondria to the cytosol was mediated by a succinate-fumarate carrier in vascular plants (Picault et al., 2004). Four putative succinate-fumarate carrier genes in IMET1 were upregulated 1.5- to 2.5-fold during the first 48 h of exposure to N- conditions (Supplemental Data Set 5).

Therefore, the evidence collectively suggests that enhanced FA and TAG synthesis under N depletion was correlated with the upregulation of transporter genes responsible for importing the intermediates (e.g., PEP and pyruvate) and ATP from the cytosol and mitochondria into the plastid and with the simultaneous downregulation of the TPT (and perhaps other related genes) to reduce the export of photosynthetic carbon precursors out of the plastid.

Carbon Fixation

Transcriptomic analysis indicated that CO_2 assimilation was severely inhibited under N- conditions: The transcriptional expression of most Calvin cycle genes was downregulated 1- to ~4-fold during the 48 h of exposure to N- conditions (Supplemental Data Set 5). Because carbon fixation efficiency can be affected by intracellular CO_2 concentrations, we examined the transcriptional dynamics of a number of genes involved in CO_2 concentration regulation mechanisms. Both carbonic anhydrase (CA)-mediated carbon-concentrating metabolism and a C4 cycle-like mechanism have previously been reported in heterokonts, including several diatoms and *Nannochloropsis* spp (Roberts et al., 2007; Kroth et al., 2008; Radakovits et al., 2012; Vieler et al., 2012). In IMET1, five putative CA genes were identified, along with two putative bicarbonate transporters and two low CO_2-inducible genes (*LCIA*) that encode a putative formate/nitrite transporter protein in the plastid envelope. The presence of CA and these inorganic carbon transporters suggests that the C4-pathway is upregulated under N deprivation conditions; alternatively, it is possible that increased CA activity may play a buffering role in balancing the carbon flux. One (g2018) of the putative CA genes and one LCIA gene (g544) were upregulated 1.5- to 2.5-fold over the 48-h exposure to N- conditions. Although all of the C4 cycle-like pathway genes, including one phosphoenolpyruvate carboxylase, three phosphate dikinases, three MEs, two malate dehydrogenases, and one phosphoenolpyruvatecarboxykinase, were identified in IMET1, their in vivo functions are puzzling because the three putative MEs (g2252, g3463, and g8325), which are the only enzymes involved in CO_2 formation in the C4-like cycle, were predicted to be localized in mitochondria and/or the cytosol, but not in the plastid (Supplemental Data Set 6). We suspected that the products of the C4 cycle-like pathway genes may be more likely to be involved in replenishing TCA cycle intermediates for lipid biosynthesis (Figure 6) than in redirecting CO_2 into the plastid for carbon fixation in IMET1.

Metabolic Regulation of Oil Synthesis in *N. oceanica*: Insights from Comparative Analysis with *C. reinhardtii*

To investigate the metabolic regulation over the TAG production under N- conditions in *N. oceanica*, we compared the gene expression features pertinent to FA synthesis and TAG assembly in IMET1 to those of several other microalgae and oil crop plants (Cagliari et al., 2010; Miller et al., 2010; Bourgis et al., 2011; Huang et al., 2011; Troncoso-Ponce et al., 2011; Boyle et al., 2012; Rismani-Yazdi et al., 2012). In IMET1, the TAG biosynthesis pathways, particularly the eukaryotic Kennedy pathway and the PDAT-mediated alternative route, were upregulated at the transcript level (Figure 4), whereas most of the genes involved in a type II FAS-based de novo FA biosynthesis in the plastid were downregulated (Figure 6; Supplemental Data Set 5). The fact that the absolute transcript levels of the FA biosynthesis enzymes were 3 to 4 times higher than those responsible for TAG synthesis suggested that the machinery for de novo FA biosynthesis is normally in excess in IMET1. Thus, the regulatory step determining final TAG concentration is the TAG assembly pathway. In other words, under N depletion, it is the upregulation of the transcript level of the key genes in TAG assembly, rather than those in FA synthesis, that leads to accelerated TAG production. A similar regulation strategy was observed in *C. reinhardtii* (Table 1) and oilseeds of *Ricinus communis*, *Brassica napus*, *Euonymus alatus*, and *Tropaeolum majus*, except *E. guineensis* (oil palm), in which FA biosynthesis rather than TAG assembly was greatly upregulated during oil accumulation (Cagliari et al., 2010; Miller et al., 2010; Bourgis et al., 2011; Huang et al., 2011; Troncoso-Ponce et al., 2011;

Table 1. Comparison of the Upregulated Genes Involved in TAG Synthesis for *N. oceanica* IMET1 and *C. reinhardtii*

Pathways	*N. oceanica* IMET1 Upregulated Genes	*C. reinhardtii* Upregulated Genes
FA synthesis and activation	FAS I, ACP, KAS (M), KAR, TE, LC-FACS	ACP, KAS I, TE, LC-FACS
TAG assembly	GPAT (E), LPAAT (E, P), PAP (E), DGAT (E, P), PDAT	PAP, DGAT, PDAT
Pyruvate production	PK (C, P), ENL (C), PGAM (C), PGK (C), GPDH (C), ALDO (C), ME (C, M)	GPI, ALDO, PGAM, PK
Acetyl-CoA production	PDHC, PDC, ALDH, ACS	PDC
Energy production	PGK (ATP), PK (ATP), GPDH (NADH), PDHC (NADH), MDH (NADH), ICDH (NADH), OGDH (NADH)	PK (ATP)

The gene expression data for *C. reinhardtii* was retrieved from the published work by Miller et al. (2010) and Boyle et al. (2012). Subcellular localization information for IMET1: M, mitochondria; E, ER membrane; P, plastid; C, cytoplasm. ACP, acyl carrier protein; ACS, acetyl-CoA synthetase; ALDO, aldolase; ENL, enolase; FAS I, type I fatty acid synthase; GPDH, glyceraldehyde-3-phosphate dehydrogenase; GPI, glucose phosphate isomerase; ICDH, isocitrate dehydrogenase; MDH, malate dehydrogenase; OGDH, 2-oxoglutarate dehydrogenase; PGAM, phosphoglycerate mutase; PGK, phosphoglycerate kinase.

Boyle et al., 2012). Although microalgae (e.g., IMET1) and many other oil crops share a similar strategy for stimulating TAG production, the genes within the TAG assembly pathway that are subject to transcriptional regulation seem to be species specific. For example, all of the genes in the Kennedy pathway, including those encoding GPAT, LPAAT, PAP, and DGAT, were under transcriptional control in IMET1 (Table 1, Figure 4; Supplemental Data Set 5), whereas only GPAT and LPAAT were regulated at the transcript level in the oleaginous green alga *Neochloris oleoabundans* (Rismani-Yazdi et al., 2012).

Although *N. oceanica* IMET1 and *C. reinhardtii* showed similar responses to N depletion with respect to plastid-associated de novo FA and TAG biosynthesis, there are several key distinctions between these two organisms. First, IMET1 possesses expressed type I FAS genes (Supplemental Data Set 5), but these genes are absent from the *C. reinhardtii* genome, suggesting that type I FAS genes may contribute additional FA for TAG synthesis in IMET1. Second, IMET1 possesses two *DGAT-1* and 11 *DGAT-2* genes, whereas *C. reinhardtii* contains only one *DGAT-1* and five *DGAT-2* genes (Boyle et al., 2012; Wang et al., 2014). Moreover, the basal level of the absolute amounts of *DGAT* transcripts was considerably higher in IMET1 (with a total FPKM value of 205.4 under N+ conditions) than in *C. reinhardtii* (with a total FPKM value of 66.4). Although the total *DGAT* transcript abundance in IMET1 increased by only ~16% during the 48-h exposure to N- conditions, which was less than that observed in *C. reinhardtii* (where *DGAT* transcript abundance increased by 62%; Boyle et al., 2012), the absolute quantities of DGAT transcripts were nevertheless considerably greater in IMET1 than in *C. reinhardtii*. Thus, the greatly increased number of copies of DGAT genes in IMET1 and the higher degree of transcript levels under both under N+ and N- conditions might have conferred the ability of IMET1 to produce considerably larger amounts of TAG under stress compared with *C. reinhardtii* and other nonoleaginous microalgae.

Previous transcriptomic and biochemical studies on microalgae and vascular plants revealed that TAG synthesis is generally limited by the supply of carbon precursors for FA synthesis (Ruuska et al., 2002; Bourgis et al., 2011; Troncoso-Ponce et al., 2011; Fan et al., 2012). Our transcriptomic analysis identified a number of pathways in IMET1 that can be stimulated under N- conditions, thereby supplying carbon precursors and energy for TAG synthesis: (1) the cytosolic glycolysis pathway, which produces pyruvate; (2) PDHC bypass, which yields additional acetyl-CoA; and (3) coupling of TCA reactions with mitochondrial β-oxidation. Five glycolysis genes (GPDH, PGK, PGAM, ENL, and PK) were upregulated in IMET1 (Table 1, Figure 6), whereas only three enzymes (phosphoglucose isomerase, fructose-1,6-bisphosphate aldolase, and phosphoglycerate mutase) were elevated in *C. reinhardtii* at the transcript level under N- conditions (Miller et al., 2010). Among the upregulated glycolytic enzymes in IMET1, PK and PGK produce ATP for FA biosynthesis, whereas these two energy-producing steps were not enhanced in *C. reinhardtii* under N- conditions. The enzymatic reaction catalyzed by ME represents another route yielding pyruvate in IMET1, which can produce both the precursor (pyruvate) and energy (NADPH) for lipid biosynthesis. In contrast to upregulation of ME in IMET1, the transcript level of ME in *C. reinhardtii* was repressed under N deprivation. Additionally, upregulation of the PDHC bypass and β-oxidation were not observed in *C. reinhardtii* cells subject to N deprivation (Miller et al., 2010). Although these genes/pathways involved in carbon precursors and TAG synthesis showed significant changes during 48 h under N deprivation, it is noteworthy that their upregulation at the transcript level was mostly moderate (<4-fold). These results indicate that the existence of additional regulatory mechanisms, such as those at the translational, posttranslational, and metabolic levels, cannot be excluded. Thus, coregulation of TAG synthesis at multiple levels is possible in this organism.

Conclusion

The concurrent global trancriptomic and lipidomic analyses conducted in this study provide a framework for better understanding glycerolipid metabolism in the oleaginous microalga *N. oceanica* IMET1. The extraordinary capability of IMET1 to produce TAG is presumably conferred by the higher gene doses of several Kennedy pathway genes (particularly *DGAT*) and higher transcript levels of these genes, compared with the nonoleaginous microalga *C. reinhardtii*. The increase in transcripts of many genes involved in carbohydrate and protein degradation along with the identification of a number of the genes encoding plastid and mitochondrial membrane transporters suggested that these pathways shunt photosynthetic carbon precursors from carbohydrate and protein metabolism into FA synthesis and ultimately TAG synthesis under nitrogen deprivation. Appropriate genetic manipulation experiments coupled with metabolic analysis are required to confirm these observations. This study also unraveled the important role of mitochondrial metabolism in TAG synthesis, which converts proteins and membrane lipids into precursors and supplies ATP and reducing equivalents (e.g., NADH) to the production of TAG. The temporal and spatial molecular model of oleaginousness, together with a large collection of gene sequences, transcriptomes, and lipidomes, should pave the way for rational genetic engineering of this and other related microalgae for the overproduction of TAG for food, feed, and biofuels.

METHODS

Design of Experimental Strategy

Nannochloropsis oceanica IMET1 was inoculated into modified f/2 liquid medium, which was prepared with 35 g L^{-1} sea salt, 1 g L^{-1} $NaNO_3$, 67 mg L^{-1} NaH_2PO_4*H_2O, 3.65 mg L^{-1} $FeCl_3$*$6H_2O$, 4.37 mg L^{-1} Na_2EDTA*$2H_2O$, trace metal mix (0.0196 mg L^{-1} $CuSO_4$*$5H_2O$, 0.0126 mg L^{-1} $NaMoO_4$*$2H_2O$, 0.044 mg L^{-1} $ZnSO_4$*$7H_2O$, 0.01 mg L^{-1} $CoCl_2$, and 0.36 mg L^{-1} $MnCl_2$*$4H_2O$), and vitamin mix (2.5 μg L^{-1} VB_{12}, 2.5 μg L^{-1} biotin, and 0.5 μg L^{-1} thiamine HCl). The algal cells were grown in liquid cultures under continuous light (~50 μmol photons m^{-2} s^{-1}) at 25°C and aerated by bubbling with a mixture of 1.5% CO_2 in air. Approximately 5 liters of algal culture in column photobioreactors was harvested by centrifugation at the linear growth phase (OD_{750} = 2.6). Cell pellets were washed three times with axenic seawater and inoculated into N-free f/2 medium (800 mL, n = 3) and f/2 medium (800 mL, n = 3) in triplicates, respectively. Cultures started with the same initial cell concentration of OD_{750} = 2.6 and were exposed to continuous illumination of 50 μmol m^{-2} s^{-1}. Cell aliquots were collected for RNA isolation after being transferred to the designated

conditions for 3, 4, 6, 12, 24, and 48 h. Three biological replicates of algal cultures were established under each of the above N+ and N- conditions, respectively.

Transcriptome Sampling and Sequencing

Total algal RNA under the above conditions was extracted using Trizol reagents (Invitrogen). For mRNA-Seq, the poly(A)-containing mRNA molecules were purified using Sera-mag Magnetic Oligo(dT) Beads (Thermo Scientific) and were fragmented into 200- to 300-bp fragments by incubation in RNA fragmentation reagent (Ambion) according to the manufacturer's instructions. The fragmented mRNA was then purified away from the fragmentation buffer using Agencourt RNAClean beads (Beckman Coulter). The purified, fragmented mRNA was converted into double-stranded cDNA using the SuperScript double-stranded cDNA synthesis kit (Invitrogen) by priming with random hexamers. Strand nonspecific transcriptome libraries were prepared using the NEBNext mRNA Library Prep Reagent Set (New England Biolabs) and sequenced for 2×90-bp runs (paired-end) using Illumina HiSequation 2000.

To ensure quality, the raw data (2×90-bp paired-end reads) were modified as follows: First, adapter pollutions in reads were deleted, and second, because the sequence qualities of Illumina reads degrade quickly toward the 3′ end, all reads were trimmed from the 3′ end until the 3′-end–most position with Phred-equivalent score was 20 or greater. The raw data were deposited in the National Center for Biotechnology Information Gene Expression Omnibus with the reference series number GSE42508. These filtered Illumina reads were aligned to the *N. oceanica* draft genome with TopHat (version 2.0.4, allowed no more than two segment mismatches) (Trapnell et al., 2009). Reads mapped to more than one location were excluded. Third, the short read mapping results from TopHat were used for the differential gene expression analysis with Cufflinks (version 2.0.4), as described below (Trapnell et al., 2010, 2013).

Estimation of Differential Gene Expression

For each of the mRNA-Seq data sets under each experimental condition, gene expression was measured as the numbers of aligned reads to annotated genes by Cufflinks (version 2.0.4) and normalized to FPKM values.

Genes were considered to be significantly differentially expressed if either of the conditions was met: (1) Their expression values showed at least a 2-fold change with a false discovery rate (FDR)-corrected P value ≤ 0.05 (Benjamini-Hochberg correction, which is provided by the Cuffdiff program in the Cufflinks package, version 2.0.4) between control and stressed conditions for at least one time point, and moreover their FPKM values at either conditions were ≥ 10. (2) Their expression values showed a 1.5- to <2-fold change with an FDR-adjusted P value ≤ 0.05 between control and stressed conditions for at least two time points, and moreover their FPKM values at either of the conditions were ≥ 10.

The 3255 differentially expressed genes were grouped into 16 clusters based on their temporal expression patterns by the *k*-means clustering using the MultiExperiment Viewer 4.8 (MeV4.8; http://www.tm4.org/mev.html) with Euclidean distance (Saeed et al., 2006). The optimal number of clusters was identified and investigated by performing a figure of merit analysis within MeV4.8 (Yeung et al., 2001). Figure of merit analysis showed that the value was stabilized after a partitioning into 12 to 18 clusters using *k*-means algorithm. Therefore, the transcripts were split into 16 clusters, each of which exhibits a particular pattern of temporal dynamics.

Validation Using Real-Time PCR

To further test the validity of the mRNA-Seq results, RNA extracted from the same cultures for mRNA-Seq was subjected to the PrimeScript RT reagent kit with gDNA Eraser (Takara) for cDNA synthesis. Also, qRT-PCR was performed by standard methods (Roche) as previously described (Guénin et al., 2009). Ct values were determined for triplicate independent technical experiments performed on triplicate biological cultures ($n = 3$). Relative fold differences were calculated based on the ΔCt method using the *actin* amplification product as an internal standard. Primer pairs used for qRT-PCR analyses are listed in Supplemental Table 2. Sizes of amplification products were 100 to 300 bp. The coefficient of determination between the qPCR results and the mRNA-Seq results was 0.94 (R^2) (Supplemental Figure 3).

Mass Spectrometry Analysis of Lipids

Ten milligrams lyophilized algal cells were homogenized in liquid nitrogen using a mortar and pestle. Total lipids were then extracted with chloroform: methanol (2:1, w/w) according to the method we previously described (Yoon et al., 2012). Lipidomic analysis was performed with an Agilent 6460 triple quadruple electrospray ionization mass spectrometer equipped with an Agilent 1260 high-performance liquid chromatograph. PC, DGTS, and PE were analyzed as $[M+H]^+$ at the positive mode of MS, while MGDG, DGDG, and TAG were detected as $[M+ NH_4]^+$; SQDG, PG, and PI were analyzed in the form of $[M-H]^-$ at the negative mode. Precursor ion and neutral loss scanning modes were employed to identify lipid species for a given class according to previously described methods (Han and Gross, 2001; Welti et al., 2002, 2003; Hsu and Turk, 2009). Product ion mode was used to resolve the acyl groups of each lipid species.

Nitrogen was used as nebulizing gas (at 0.3 Bar) and a dry gas (4 liters min^{-1} at 200°C). The spray capillary voltage was 3700 V for the negative ion mode and 4200 V for the positive ion mode. Internal standards, including PC 17:0/20:4 (Avanti Polar Lipids), PE14:1/17:0 (Avanti Polar Lipids), MGDG 18:0/18:0 (Matreya), DGDG 18:0/18:0 (Matreya), TAG 17:0/17:0/17:0 (Sigma-Aldrich), PG 17:0/20:4 (Avanti Polar Lipids), and PI 17:0/20:4 (Avanti Polar Lipids), were added to the lipid extract prior to mass spectrometry analysis. Lipid extracts were separated at 40°C on a ZOBAX SBC18 column (1.8 μm, 2.1× 150 mm; Agilent) and an Extend C18 column (1.8 μm, 2.1× 150 mm; Agilent) for positive- and negative-mode mass spectrometry analysis, respectively. For positive mode, the mobile phases were methanol:acetonitrile:water (19:19:2) (A) and isoproponal (B) containing 0.1% formic acid and 10 mM ammonium acetate; the LC gradients were as follows: 0 min, 90% A and 10% B; 5 min, 90% A and 10% B; 25 min, 60% A and 40% B; 60 min, 45% A and 55% B; 66 min, 45% A and 55% B; and 68 min, 90% A and 10% B. For negative mode, the mobile phases were 85% methanol (A) and isopropanol containing 0.025% NH_4OH; the LC gradients were as follows: 0 min, 95% A and 5% B; 15 min, 85% A and 15% B, 22 min, 45% A and 55% B; 42 min, 45% A and 55% B; and 44 min, 95% A and 5% B. The flow rate was 0.2 mL min^{-1}. Multiple reaction monitoring scanning mode was used for mass spectrometry detection: PC ($[M+H]^+ \rightarrow m/z$ 184), DGTS ($[M+H]^+ \rightarrow m/z$ 236), PE ($[M+H]^+ \rightarrow [M+H-141]^+$), PG ($[M-H]^- \rightarrow m/z$ 153), and SQDG ($[M-H]^- \rightarrow$ m/z 225, PI ($[M-H]^+ \rightarrow m/z$ 241). For MGDG, DGDG, and TAG, single-stage mass spectrometry scanning mode was employed for detection of $[M+NH_4]^+$. For quantification, calibration standards of each lipid class were titrated relative to a constant amount of internal standard. Relative intensity ratios were plotted against their molar concentration ratios to establish standard curves. The calibration standards included PC 18:1/18:1, DGTS 16:0/16:0, PE 18:0/18:1, MGDG 16:3/18:3, DGDG, PI 18:1/18:1, PG 18:0/18:1 (all from Avanti Polar Lipids); SQDG 16:0/18:3 (Indofine Chemical); and TAG 16:1/16:1/16:1, TAG 16:0/18:1/16:0, TAG 18:1/16:0/18:1, and TAG 18:1/18:1/18:1 (all from Sigma-Aldrich).

Fold change of the lipid content in response to N deprivation was calculated as $\log_2$(lc(Tx, N-)/lc (Tx, N+)) (lc = content of lipid species, Tx = time point, N- = N deprivation, N+ = N-replete) and displayed as a heat map. Student's *t* test was used to compare the two data sets (N-deprived and N-replete, $n = 6$) at the same time point. If the test gives a P value ≤ 0.01, the difference between N- and N+ was interpreted as being significant.

Accession Numbers

The mRNA-Seq data from this article can be found in the National Center for Biotechnology Information Gene Expression Omnibus under accession number GSE42508. Accession numbers for the *N. oceanica* IMET1 genes were also included in Supplemental Data Sets 2, 4, 5, and 6.

Supplemental Data

The following materials are available in the online version of this article.

Supplemental Figure 1. Growth Curves of IMET1 Cells under N+ and N- Conditions.

Supplemental Figure 2. Clustering Analysis of the mRNA-Seq–Based Time-Series Transcriptome Data Set.

Supplemental Figure 3. Consistency between mRNA-Seq–Based and Real-Time PCR–Based Transcript Quantification.

Supplemental Figure 4. Transcript Abundance and Dynamics of the DGAT Genes in IMET1 as Measured by mRNA-Seq and Real-Time Quantitative PCR.

Supplemental Table 1. General Information of the mRNA-Seq Data.

Supplemental Table 2. Real-Time PCR Primer Sequences for the 13 Genes Used in Real-Time PCR Experiments to Validate the mRNA-Seq Results.

Supplemental Data Set 1. Spearman Correlation of Transcript Profiles.

Supplemental Data Set 2. The mRNA-Seq Data for the 3255 Differentially Expressed Genes and Manual Functional Curation.

Supplemental Data Set 3. Cellular Content of the 55 Glycerolipid Molecular Species under N+ and N- Conditions.

Supplemental Data Set 4. Protein Sequences of *N. oceanica* IMET1 Genes Related to TAG and Lipid Synthesis.

Supplemental Data Set 5. The mRNA-Seq Data for the Genes Involved in Glycerolipid Metabolism, Fatty Acid Biosynthesis, Lipases, Carbon Fixation and CCM, Carbon Metabolism and Transporter, and β-Oxidation.

Supplemental Data Set 6. Subcellular Localization Prediction for the Selected Putative Proteins Involved in TAG Synthesis and Carbon Metabolism.

ACKNOWLEDGMENTS

This work was supported by the Ministry of Science and Technology of China (2012CB721101 and 2012AA02A707), the International Research Collaboration Program (31010103907), and the Young Investigator Program (61103167) from National Natural Science Foundation of China and International Innovation Partnership Program and Solar Energy Research Initiative from Chinese Academy of Sciences. No competing interests are declared. The RNA-Seq data were deposited as GSE42508 at the Gene Expression Omnibus database.

AUTHOR CONTRIBUTIONS

J.X. and Q.H. designed the research. J.L., L.W., X.J., and J.C. cultivated algae and characterized the transcriptome. D.H. and J.J. characterized the lipidome. K.N. and S.H. contributed computational tools. J.L., D.H., D.W., Y. L, Q.H., and J.X. analyzed the data. J.X., Q.H., J.L., and D.H. wrote the article.

Received December 16, 2013; revised February 16, 2014; accepted March 11, 2014; published April 1, 2014.

REFERENCES

Alonso, A.P., Goffman, F.D., Ohlrogge, J.B., and Shachar-Hill, Y. (2007). Carbon conversion efficiency and central metabolic fluxes in developing sunflower (*Helianthus annuus* L.) embryos. Plant J. **52:** 296–308.

Bates, P.D., Durrett, T.P., Ohlrogge, J.B., and Pollard, M. (2009). Analysis of acyl fluxes through multiple pathways of triacylglycerol synthesis in developing soybean embryos. Plant Physiol. **150:** 55–72.

Bates, P.D., Ohlrogge, J.B., and Pollard, M. (2007). Incorporation of newly synthesized fatty acids into cytosolic glycerolipids in pea leaves occurs via acyl editing. J. Biol. Chem. **282:** 31206–31216.

Beattie, A., Hirst, E.L., and Percival, E. (1961). Studies on the metabolism of the Chrysophyceae. Comparative structural investigations on leucosin (chrysolaminarin) separated from diatoms and laminarin from the brown algae. Biochem. J. **79:** 531–537.

Bourgis, F., Kilaru, A., Cao, X., Ngando-Ebongue, G.F., Drira, N., Ohlrogge, J.B., and Arondel, V. (2011). Comparative transcriptome and metabolite analysis of oil palm and date palm mesocarp that differ dramatically in carbon partitioning. Proc. Natl. Acad. Sci. USA **108:** 12527–12532.

Boyle, N.R., et al. (2012). Three acyltransferases and nitrogen-responsive regulator are implicated in nitrogen starvation-induced triacylglycerol accumulation in *Chlamydomonas.* J. Biol. Chem. **287:** 15811–15825.

Browse, J., Kunst, L., Anderson, S., Hugly, S., and Somerville, C. (1989). A mutant of Arabidopsis deficient in the chloroplast 16:1/18:1 desaturase. Plant Physiol. **90:** 522–529.

Browse, J., McCourt, P., and Somerville, C.R. (1985). A mutant of Arabidopsis lacking a chloroplast-specific lipid. Science **227:** 763–765.

Buléon, A., Gallant, D.J., Bouchet, B., Mouille, G., D'Hulst, C., Kossmann, J., and Ball, S. (1997). Starches from A to C. *Chlamydomonas reinhardtii* as a model microbial system to investigate the biosynthesis of the plant amylopectin crystal. Plant Physiol. **115:** 949–957.

Cagliari, A., Margis-Pinheiro, M., Loss, G., Mastroberti, A.A., de Araujo Mariath, J.E., and Margis, R. (2010). Identification and expression analysis of castor bean (*Ricinus communis*) genes encoding enzymes from the triacylglycerol biosynthesis pathway. Plant Sci. **179:** 499–509.

Carpinelli, E.C., Telatin, A., Vitulo, N., Forcato, C., D'Angelo, M., Schiavon, R., Vezzi, A., Giacometti, G.M., Morosinotto, T., and Valle, G. (2013). Chromosome scale genome assembly and transcriptome profiling of *Nannochloropsis gaditana* in nitrogen depletion. Mol Plant **6,** sst120v122-sst120.

Chapman, K.D., and Ohlrogge, J.B. (2012). Compartmentation of triacylglycerol accumulation in plants. J. Biol. Chem. **287:** 2288–2294.

Claros, M.G. (1995). MitoProt, a Macintosh application for studying mitochondrial proteins. Comput. Appl. Biosci. **11:** 441–447.

Coleman, R.A., and Lee, D.P. (2004). Enzymes of triacylglycerol synthesis and their regulation. Prog. Lipid Res. **43:** 134–176.

Dong, H.P., Williams, E., Wang, D.Z., Xie, Z.X., Hsia, R.C., Jenck, A., Halden, R., Li, J., Chen, F., and Place, A.R. (2013). Responses of *Nannochloropsis oceanica* IMET1 to long-term nitrogen starvation and recovery. Plant Physiol. **162:** 1110–1126.

Dunahay, T.G., Jarvis, E.E., and Roessler, P.G. (1995). Genetic transformation of the diatoms *Cyclotella cryptica* and *Navicula saprophila.* J. Phycol. **31:** 1004–1012.

Emanuelsson, O., Nielsen, H., and von Heijne, G. (1999). ChloroP, a neural network-based method for predicting chloroplast transit peptides and their cleavage sites. Protein Sci. **8:** 978–984.

Fan, J.L., Andre, C., and Xu, C.C. (2011). A chloroplast pathway for the de novo biosynthesis of triacylglycerol in *Chlamydomonas reinhardtii.* FEBS Lett. **585:** 1985–1991.

Fan, J.L., Yan, C.S., Andre, C., Shanklin, J., Schwender, J., and Xu, C.C. (2012). Oil accumulation is controlled by carbon precursor supply for fatty acid synthesis in *Chlamydomonas reinhardtii.* Plant Cell Physiol. **53:** 1380–1390.

Fischer, K., Kammerer, B., Gutensohn, M., Arbinger, B., Weber, A., Häusler, R.E., and Flügge, U.I. (1997). A new class of plastidic phosphate translocators: a putative link between primary and secondary metabolism by the phosphoenolpyruvate/phosphate antiporter. Plant Cell **9:** 453–462.

Flügge, U.I., Häusler, R.E., Ludewig, F., and Gierth, M. (2011). The role of transporters in supplying energy to plant plastids. J. Exp. Bot. **62:** 2381–2392.

Frentzen, M. (1998). Acyltransferases from basic science to modified seed oils. Lipid/Fett **100:** 161–166.

Fulda, M., Shockey, J., Werber, M., Wolter, F.P., and Heinz, E. (2002). Two long-chain acyl-CoA synthetases from *Arabidopsis thaliana* involved in peroxisomal fatty acid beta-oxidation. Plant J. **32:** 93–103.

Furumoto, T., et al. (2011). A plastidial sodium-dependent pyruvate transporter. Nature **476:** 472–475.

Gao, J., Ajjawi, I., Manoli, A., Sawin, A., Xu, C., Froehlich, J.E., Last, R.L., and Benning, C. (2009). FATTY ACID DESATURASE4 of Arabidopsis encodes a protein distinct from characterized fatty acid desaturases. Plant J. **60:** 832–839.

Georgianna, D.R., and Mayfield, S.P. (2012). Exploiting diversity and synthetic biology for the production of algal biofuels. Nature **488:** 329–335.

Gerhardt, B. (1992). Fatty acid degradation in plants. Prog. Lipid Res. **31:** 417–446.

Gibbs, S.P. (1979). The route of entry of cytoplasmically synthesized proteins into chloroplasts of algae possessing chloroplast ER. J. Cell Sci. **35:** 253–266.

Goodson, C., Roth, R., Wang, Z.T., and Goodenough, U. (2011). Structural correlates of cytoplasmic and chloroplast lipid body synthesis in *Chlamydomonas reinhardtii* and stimulation of lipid body production with acetate boost. Eukaryot. Cell **10:** 1592–1606.

Gschloessl, B., Guermeur, Y., and Cock, J.M. (2008). HECTAR: A method to predict subcellular targeting in heterokonts. BMC Bioinformatics **9:** 393.

Gueguen, V., Macherel, D., Jaquinod, M., Douce, R., and Bourguignon, J. (2000). Fatty acid and lipoic acid biosynthesis in higher plant mitochondria. J. Biol. Chem. **275:** 5016–5025.

Guénin, S., Mauriat, M., Pelloux, J., Van Wuytswinkel, O., Bellini, C., and Gutierrez, L. (2009). Normalization of qRT-PCR data: the necessity of adopting a systematic, experimental conditions-specific, validation of references. J. Exp. Bot. **60:** 487–493.

Han, X., and Gross, R.W. (2001). Quantitative analysis and molecular species fingerprinting of triacylglyceride molecular species directly from lipid extracts of biological samples by electrospray ionization tandem mass spectrometry. Anal. Biochem. **295:** 88–100.

Heilmann, I., Mekhedov, S., King, B., Browse, J., and Shanklin, J. (2004). Identification of the *Arabidopsis* palmitoyl-monogalactosyldiacylglycerol delta7-desaturase gene FAD5, and effects of plastidial retargeting of *Arabidopsis* desaturases on the fad5 mutant phenotype. Plant Physiol. **136:** 4237–4245.

Hockin, N.L., Mock, T., Mulholland, F., Kopriva, S., and Malin, G. (2012). The response of diatom central carbon metabolism to nitrogen starvation is different from that of green algae and higher plants. Plant Physiol. **158:** 299–312.

Hsu, F.F., and Turk, J. (2009). Electrospray ionization with low-energy collisionally activated dissociation tandem mass spectrometry of glycerophospholipids: Mechanisms of fragmentation and structural characterization. J. Chromatogr. B Analyt. Technol. Biomed. Life Sci. **877:** 2673–2695.

Hu, Q., Sommerfeld, M., Jarvis, E., Ghirardi, M., Posewitz, M., Seibert, M., and Darzins, A. (2008). Microalgal triacylglycerols as feedstocks for biofuel production: Perspectives and advances. Plant J. **54:** 621–639.

Huang, J.Y., Jie, Z.J., Wang, L.J., Yan, X.H., and Wei, W.H. (2011). Analysis of the differential expression of the genes related to *Brassica napus* seed development. Mol. Biol. Rep. **38:** 1055–1061.

Iba, K., Gibson, S., Nishiuchi, T., Fuse, T., Nishimura, M., Arondel, V., Hugly, S., and Somerville, C. (1993). A gene encoding a chloroplast omega-3 fatty acid desaturase complements alterations in fatty acid desaturation and chloroplast copy number of the fad7 mutant of *Arabidopsis thaliana.* J. Biol. Chem. **268:** 24099–24105.

Joyard, J., Ferro, M., Masselon, C., Seigneurin-Berny, D., Salvi, D., Garin, J., and Rolland, N. (2010). Chloroplast proteomics highlights the subcellular compartmentation of lipid metabolism. Prog. Lipid Res. **49:** 128–158.

Kachroo, A., Shanklin, J., Whittle, E., Lapchyk, L., Hildebrand, D., and Kachroo, P. (2007). The Arabidopsis stearoyl-acyl carrier protein-desaturase family and the contribution of leaf isoforms to oleic acid synthesis. Plant Mol. Biol. **63:** 257–271.

Kang, F., and Rawsthorne, S. (1996). Metabolism of glucose-6-phosphate and utilization of multiple metabolites for fatty acid synthesis by plastids from developing oilseed rape embryos. Planta **199:** 321–327.

Kaup, M.T., Froese, C.D., and Thompson, J.E. (2002). A role for diacylglycerol acyltransferase during leaf senescence. Plant Physiol. **129:** 1616–1626.

Koo, A.J., Ohlrogge, J.B., and Pollard, M. (2004). On the export of fatty acids from the chloroplast. J. Biol. Chem. **279:** 16101–16110.

Kroth, P.G., et al. (2008). A model for carbohydrate metabolism in the diatom *Phaeodactylum tricornutum* deduced from comparative whole genome analysis. PLoS ONE **3:** e1426.

Kunau, W.H., Dommes, V., and Schulz, H. (1995). beta-oxidation of fatty acids in mitochondria, peroxisomes, and bacteria: A century of continued progress. Prog. Lipid Res. **34:** 267–342.

Lassner, M.W., Levering, C.K., Davies, H.M., and Knutzon, D.S. (1995). Lysophosphatidic acid acyltransferase from meadowfoam mediates insertion of erucic acid at the sn-2 position of triacylglycerol in transgenic rapeseed oil. Plant Physiol. **109:** 1389–1394.

León-Bañares, R., González-Ballester, D., Galván, A., and Fernández, E. (2004). Transgenic microalgae as green cell-factories. Trends Biotechnol. **22:** 45–52.

Li, X.B., Moellering, E.R., Liu, B.S., Johnny, C., Fedewa, M., Sears, B.B., Kuo, M.H., and Benning, C. (2012). A galactoglycerolipid lipase is required for triacylglycerol accumulation and survival following nitrogen deprivation in *Chlamydomonas reinhardtii.* Plant Cell **24:** 4670–4686.

Li, Y., Han, D., Sommerfeld, M., and Hu, Q. (2011). Photosynthetic carbon partitioning and lipid production in the oleaginous microalga *Pseudochlorococcum sp.* (Chlorophyceae) under nitrogen-limited conditions. Bioresour. Technol. **102:** 123–129.

Li, Y.T., Han, D.X., Hu, G.R., Dauvillee, D., Sommerfeld, M., Ball, S., and Hu, Q. (2010a). *Chlamydomonas* starchless mutant defective in ADP-glucose pyrophosphorylase hyper-accumulates triacylglycerol. Metab. Eng. **12:** 387–391.

Li, Y.T., Han, D.X., Hu, G.R., Sommerfeld, M., and Hu, Q.A. (2010b). Inhibition of starch synthesis results in overproduction of lipids in *Chlamydomonas reinhardtii.* Biotechnol. Bioeng. **107:** 258–268.

Li-Beisson, Y., et al. (2010). Acyl-lipid metabolism. Arabidopsis Book **8:** e0133, doi/10.1199/tab.0133.

Lin, M., Behal, R., and Oliver, D.J. (2003). Disruption of plE2, the gene for the E2 subunit of the plastid pyruvate dehydrogenase complex, in Arabidopsis causes an early embryo lethal phenotype. Plant Mol. Biol. **52:** 865–872.

Lutziger, I., and Oliver, D.J. (2000). Molecular evidence of a unique lipoamide dehydrogenase in plastids: analysis of plastidic lipoamide dehydrogenase from *Arabidopsis thaliana.* FEBS Lett. **484:** 12–16.

Masterson, C., and Wood, C. (2001). Mitochondrial and peroxisomal beta-oxidation capacities of organs from a non-oilseed plant. Proc. Biol. Sci. **268:** 1949–1953.

Matos, A.R., d'Arcy-Lameta, A., França, M., Pêtres, S., Edelman, L., Kader, J.C., Zuily-Fodil, Y., and Pham-Thi, A.T. (2001). A novel patatin-like gene stimulated by drought stress encodes a galactolipid acyl hydrolase. FEBS Lett. **491:** 188–192.

Matos, A.R., d'Arcy-Lameta, A., França, M., Zuily-Fodil, Y., and Pham-Thi, A.T. (2000). A patatin-like protein with galactolipase activity is induced by drought stress in *Vigna unguiculata* leaves. Biochem. Soc. Trans. **28:** 779–781.

Merchant, S.S., Kropat, J., Liu, B.S., Shaw, J., and Warakanont, J. (2012). TAG, you're it! Chlamydomonas as a reference organism for understanding algal triacylglycerol accumulation. Curr. Opin. Biotechnol. **23:** 352–363.

Merchant, S.S., et al. (2007). The *Chlamydomonas* genome reveals the evolution of key animal and plant functions. Science **318:** 245–250.

Miller, R., et al. (2010). Changes in transcript abundance in *Chlamydomonas reinhardtii* following nitrogen deprivation predict diversion of metabolism. Plant Physiol. **154:** 1737–1752.

Ohlrogge, J., and Browse, J. (1995). Lipid biosynthesis. Plant Cell **7:** 957–970.

Oliver, D.J., Nikolau, B.J., and Wurtele, E.S. (2009). Acetyl-CoA-Life at the metabolic nexus. Plant Sci. **176:** 597–601.

Petersen, T.N., Brunak, S., von Heijne, G., and Nielsen, H. (2011). SignalP 4.0: Discriminating signal peptides from transmembrane regions. Nat. Methods **8:** 785–786.

Picault, N., Hodges, M., Palmieri, L., and Palmieri, F. (2004). The growing family of mitochondrial carriers in Arabidopsis. Trends Plant Sci. **9:** 138–146.

Plaxton, W.C. (1996). The organization and regulation of plant glycolysis. Annu. Rev. Plant Physiol. Plant Mol. Biol. **47:** 185–214.

Radakovits, R., Jinkerson, R.E., Fuerstenberg, S.I., Tae, H., Settlage, R.E., Boore, J.L., and Posewitz, M.C. (2012). Draft genome sequence and genetic transformation of the oleaginous alga *Nannochloropis gaditana.* Nat. Commun. **3:** 686.

Rawsthorne, S. (2002). Carbon flux and fatty acid synthesis in plants. Prog. Lipid Res. **41:** 182–196.

Rismani-Yazdi, H., Haznedaroglu, B.Z., Hsin, C., and Peccia, J. (2012). Transcriptomic analysis of the oleaginous microalga *Neochloris oleoabundans* reveals metabolic insights into triacylglyceride accumulation. Biotechnol. Biofuels **5:** 74.

Roberts, K., Granum, E., Leegood, R.C., and Raven, J.A. (2007). C3 and C4 pathways of photosynthetic carbon assimilation in marine diatoms are under genetic, not environmental, control. Plant Physiol. **145:** 230–235.

Roesler, K., Shintani, D., Savage, L., Boddupalli, S., and Ohlrogge, J. (1997). Targeting of the Arabidopsis homomeric acetyl-coenzyme A carboxylase to plastids of rapeseeds. Plant Physiol. **113:** 75–81.

Roessler, P.G. (1987). UDP-glucose pyrophosphorylase activity in the diatom *Cyclotella cryptica* - Pathway of chrysolaminarin biosynthesis. J. Phycol. **23:** 494–498.

Roessler, P.G. (1988). Changes in the activities of various lipid and carbohydrate biosynthetic enzymes in the diatom *Cyclotella cryptica* in response to silicon deficiency. Arch. Biochem. Biophys. **267:** 521–528.

Rosenberg, J.N., Oyler, G.A., Wilkinson, L., and Betenbaugh, M.J. (2008). A green light for engineered algae: Redirecting metabolism to fuel a biotechnology revolution. Curr. Opin. Biotechnol. **19:** 430–436.

Roughan, P.G., and Ohlrogge, J.B. (1994). On the assay of acetyl-CoA synthetase activity in chloroplasts and leaf extracts. Anal. Biochem. **216:** 77–82.

Ruuska, S.A., Girke, T., Benning, C., and Ohlrogge, J.B. (2002). Contrapuntal networks of gene expression during Arabidopsis seed filling. Plant Cell **14:** 1191–1206.

Saeed, A.I., Bhagabati, N.K., Braisted, J.C., Liang, W., Sharov, V., Howe, E.A., Li, J.W., Thiagarajan, M., White, J.A., and Quackenbush, J. (2006). TM4 microarray software suite. Methods Enzymol. **411:** 134–193.

Schultz, D.J., Suh, M.C., and Ohlrogge, J.B. (2000). Stearoyl-acyl carrier protein and unusual acyl-acyl carrier protein desaturase activities are differentially influenced by ferredoxin. Plant Physiol. **124:** 681–692.

Schwender, J., Shachar-Hill, Y., and Ohlrogge, J.B. (2006). Mitochondrial metabolism in developing embryos of *Brassica napus.* J. Biol. Chem. **281:** 34040–34047.

Simionato, D., Block, M.A., La Rocca, N., Jouhet, J., Maréchal, E., Finazzi, G., and Morosinotto, T. (2013). The response of *Nannochloropsis gaditana* to nitrogen starvation includes *de novo* biosynthesis of triacylglycerols, a decrease of chloroplast galactolipids, and reorganization of the photosynthetic apparatus. Eukaryot. Cell **12:** 665–676.

Stone, S.J., Levin, M.C., Zhou, P., Han, J., Walther, T.C., and Farese, R.V., Jr.,. (2009). The endoplasmic reticulum enzyme DGAT2 is found in mitochondria-associated membranes and has a mitochondrial targeting signal that promotes its association with mitochondria. J. Biol. Chem. **284:** 5352–5361.

Sukenik, A. (1991). Ecophysiological considerations in the pptimization of eicosapentaenoic acid production by *Nannochloropsis* sp. (Eustigmatophyceae). Bioresour. Technol. **35:** 263–269.

Sweetlove, L.J., Beard, K.F.M., Nunes-Nesi, A., Fernie, A.R., and Ratcliffe, R.G. (2010). Not just a circle: Flux modes in the plant TCA cycle. Trends Plant Sci. **15:** 462–470.

Trapnell, C., Hendrickson, D.G., Sauvageau, M., Goff, L., Rinn, J.L., and Pachter, L. (2013). Differential analysis of gene regulation at transcript resolution with RNA-seq. Nat. Biotechnol. **31:** 46–53.

Trapnell, C., Pachter, L., and Salzberg, S.L. (2009). TopHat: Discovering splice junctions with RNA-Seq. Bioinformatics **25:** 1105–1111.

Trapnell, C., Williams, B.A., Pertea, G., Mortazavi, A., Kwan, G., van Baren, M.J., Salzberg, S.L., Wold, B.J., and Pachter, L. (2010). Transcript assembly and quantification by RNA-Seq reveals unannotated transcripts and isoform switching during cell differentiation. Nat. Biotechnol. **28:** 511–515.

Troncoso-Ponce, M.A., Kilaru, A., Cao, X., Durrett, T.P., Fan, J.L., Jensen, J.K., Thrower, N.A., Pauly, M., Wilkerson, C., and Ohlrogge, J.B. (2011). Comparative deep transcriptional profiling of four developing oilseeds. Plant J. **68:** 1014–1027.

Venglat, P., et al. (2011). Gene expression analysis of flax seed development. BMC Plant Biol. **11:** 74.

Vieler, A., et al. (2012). Genome, functional gene annotation, and nuclear transformation of the heterokont oleaginous alga *Nannochloropsis oceanica* CCMP1779. PLoS Genet. **8:** e1003064.

Wada, H., Shintani, D., and Ohlrogge, J. (1997). Why do mitochondria synthesize fatty acids? Evidence for involvement in lipoic acid production. Proc. Natl. Acad. Sci. USA **94:** 1591–1596.

Wang, D.M., Lu, Y.D., Huang, H., and Xu, J. (2012). Establishing oleaginous microalgae research models for consolidated bioprocessing of solar energy. Adv. Biochem. Eng. Biotechnol. **128:** 69–84.

Wang, D.M., et al. (2014). *Nannochloropsis* genomes reveal evolution of microalgal oleaginous traits. PLoS Genet. **10:** e1004094.

Weber, A.P., and Linka, N. (2011). Connecting the plastid: transporters of the plastid envelope and their role in linking plastidial with cytosolic metabolism. Annu. Rev. Plant Biol. **62:** 53–77.

Wei, L., Xin, Y., Wang, D.M., Jing, X.Y., Zhou, Q., Su, X.Q., Jia, J., Ning, K., Chen, F., Hu, Q., and Xu, J. (2013). Nannochloropsis plastid and mitochondrial phylogenomes reveal organelle diversification mechanism and intragenus phylotyping strategy in microalgae. BMC Genomics **14:** 534.

Welti, R., Li, W., Li, M., Sang, Y., Biesiada, H., Zhou, H.E., Rajashekar, C.B., Williams, T.D., and Wang, X. (2002). Profiling membrane lipids in plant stress responses. Role of phospholipase D alpha in freezing-induced lipid changes in *Arabidopsis.* J. Biol. Chem. **277:** 31994–32002.

Welti, R., Wang, X., and Williams, T.D. (2003). Electrospray ionization tandem mass spectrometry scan modes for plant chloroplast lipids. Anal. Biochem. **314:** 149–152.

Work, V.H., Radakovits, R., Jinkerson, R.E., Meuser, J.E., Elliott, L.G., Vinyard, D.J., Laurens, L.M.L., Dismukes, G.C., and Posewitz, M.C. (2010). Increased lipid accumulation in the *Chlamydomonas reinhardtii* sta7-10 starchless isoamylase mutant and increased carbohydrate synthesis in complemented strains. Eukaryot. Cell **9:** 1251–1261.

Xiao, Y., Zhang, J.T., Cui, J.T., Feng, Y.G., and Cui, Q. (2013). Metabolic profiles of *Nannochloropsis oceanica* IMET1 under nitrogen-deficiency stress. Bioresour. Technol. **130:** 731–738.

Yang, W.Y., Devaiah, S.P., Pan, X.Q., Isaac, G., Welti, R., and Wang, X.M. (2007). AtPLAI is an acyl hydrolase involved in basal jasmonic acid production and Arabidopsis resistance to *Botrytis cinerea.* J. Biol. Chem. **282:** 18116–18128.

Yasuno, R., von Wettstein-Knowles, P., and Wada, H. (2004). Identification and molecular characterization of the beta-ketoacyl-[acyl carrier protein] synthase component of the Arabidopsis mitochondrial fatty acid synthase. J. Biol. Chem. **279:** 8242–8251.

Yeung, K.Y., Haynor, D.R., and Ruzzo, W.L. (2001). Validating clustering for gene expression data. Bioinformatics **17:** 309–318.

Yoon, K., Han, D., Li, Y., Sommerfeld, M., and Hu, Q. (2012). Phospholipid:diacylglycerol acyltransferase is a multifunctional enzyme involved in membrane lipid turnover and degradation while synthesizing triacylglycerol in the unicellular green microalga *Chlamydomonas reinhardtii.* Plant Cell **24:** 3708–3724.

Zhao, L., Katavic, V., Li, F., Haughn, G.W., and Kunst, L. (2010). Insertional mutant analysis reveals that long-chain acyl-CoA synthetase 1 (LACS1), but not LACS8, functionally overlaps with LACS9 in Arabidopsis seed oil biosynthesis. Plant J. **64:** 1048–1058.

Zheng, M.G., Tian, J.H., Yang, G.P., Zheng, L., Chen, G.G., Chen, J.L., and Wang, B. (2013). Transcriptome sequencing, annotation and expression analysis of *Nannochloropsis sp*. at different growth phases. Gene **523:** 117–121.